TiO_2 photocatalysis for the degradation of pollutants in gas phase : from morphological design to plasmonic enhancement

TiO_2 photocatalysis for the degradation of pollutants in gas phase: from morphological design to plasmonic enhancement

Sammy W. Verbruggen [a,b]*

[a] Sustainable Energy, Air & Water Technology (DuEL), Department of Bioscience Engineering, University of Antwerp, Groenenborgerlaan 171, 2020 Antwerp, Belgium

[b] Center for Surface Chemistry and Catalysis, Department of Microbial and Molecular Systems, KU Leuven, Kasteelpark Arenberg 23, 3001 Heverlee (Leuven), Belgium

* Corresponding author: Sammy.verbruggen@uantwerpen.be

Tel: +32 3 265 32 60, Fax: +32 3 265 32 25

ABSTRACT

TiO_2-based photocatalysis has become a viable technology in various application fields such as (waste)water purification, photovoltaics/artificial photosynthesis, environmentally friendly organic synthesis and remediation of air pollution. Because of the increasing impact of bad air quality worldwide, this review focuses on the use and optimization of TiO_2-based photocatalysts for gas phase applications. Over the past years various specific aspects of TiO_2 photocatalysis have been reviewed individually. The intent of this review is to offer a broad tutorial on (recent) trends in TiO_2 photocatalyst modification for the intensification of photocatalytic air treatment. After briefly introducing the fundamentals of photocatalysis, TiO_2 photocatalyst modification is discussed both on a morphological as well as an electronic level from the perspective of gas phase applications. The main focus is laid on recent developments, but also possible opportunities to the field. This review is intended as a solid introduction for researchers new to the field, as well as a summarizing update for established investigators.

Keywords: Photocatalysis; titanium dioxide; gas phase; modification; morphology; plasmon

TABLE OF CONTENTS

1 INTRODUCTION: IMPORTANCE OF AIR CLEANING

Robert Orben, an American comedy writer once said: *"There's so much pollution in the air now, that if it weren't for our lungs there'd be no place to put it all"*. Unfortunately, some truth can be found in his playful words. As an illustration: for 2008 the World Health Organization (WHO) published a world map indicating the number of deaths caused by poor outdoor air quality (Figure 1). In a recent press release they claimed that in 2012 one out of eight deaths worldwide can be linked to air pollution.[1] Also the European Environment Agency (EEA) has published data on the statistical life expectancy reduction due to high levels of airborne pollutants. In their 2012 air quality report it is stated that human life expectancy is reduced by more than eight months on average and by more than two years in the most polluted cities and regions.[2] Though this is a controversial statement, it clearly indicates that air pollution is a serious problem that calls for urgent action from policy makers (e.g. by developing concise guidelines and enforcing realistic exposure levels), as well as from scientists by investigating sustainable environmental solutions.

Indoor air quality is often even worse that outdoor air quality. Indoor air pollution levels are roughly the same as those outdoors *plus* additional contaminants from indoor sources. Preventing pollution by source oriented measures is obviously the most convenient way of improving air quality levels, but it is utopia to believe that this alone will solve the problem. In case these primary measures are not sufficient, secondary measures need to be considered. For instance increased ventilation of confined spaces is frequently used to reduce pollutant levels indoors, but this merely transfers the contaminants to another location.[3,4] Purifiers based on filters or adsorbents can successfully remove harmful

components from the air, but the net effect is a mere transfer from one phase to another.[3,5] Therefore direct abatement of airborne contaminants is one of the more interesting options. A number of advanced oxidation processes (AOPs) have been proposed to serve as viable air cleaning technologies. AOPs are chemical oxidation reactions that exploit the high reactivity of oxygen (more specifically hydroxyl (•OH)) radicals.[6] Air-based AOPs include ozonation, often combined with H_2O_2, a catalyst or UV irradiation,[7,8] and photocatalytic oxidation (PCO). PCO offers the advantage that there is no need for additional chemicals such as H_2O_2 and there are basically no waste streams.

The first accounts on gas-solid heterogeneous photocatalysis can be traced back to the 1970's with the work of Teichner's and Stone's groups.[9–11] Since then the use of photocatalysis in gaseous systems has been investigated with exponential interest, especially during the last two decades (Figure 2). In these studies, titanium dioxide (TiO_2) is the most encountered photocatalyst, because it is considered inexpensive, (photo)stable, non-toxic, and easily activated by (near-)UV light.[12]

This review focuses on the use and optimization of TiO_2-based photocatalysts for gas phase applications. At this point it is important to stress that although this review is written from the perspective of air purification, photocatalysis is also a promising technology in the fields of (waste)water purification,[13–15] photovoltaics/artificial photosynthesis[16,17] and environmentally friendly organic synthesis.[18–20] Given the vast amount of information available on the topic, it is impossible to include *all* contributions to the field. In addition, many different aspects of TiO_2 photocatalysis and catalyst modification have been reviewed individually. The intent of this review is to offer a broad overview of trends in TiO_2 photocatalyst modification, both on a morphologic as well as electronic level, for the intensification of photocatalytic applications in the gas phase. The text is illustrated with validated results from literature and some recent results of our group. Where applicable, more detailed (review) articles will be suggested to the reader for further reference.

2 TARGETING THE POLLUTANTS

Against expectation, pollutant levels indoors are often higher than outside (EPA, 2013), due to recent building techniques where better insulation is not always compensated by sufficient ventilation. This led to new symptomatic diseases such as "sick building syndrome", characterized by headaches, nausea and irritation of skin, eyes, nose and throat.[21] Fortunately, many of the airborne contaminants can be destroyed by PCO. The most important classes of outdoor and indoor gaseous (in)organic contaminants amenable to PCO by TiO_2-based photocatalysts, are nitric oxides (NO_x), sulfur oxides (SO_x), volatile organic compounds (VOCs) and dioxins, as illustrated in Table 1. With regard to this table, note that the booming field of gas phase photocatalysis has led to the development of a

myriad of photoreactors and testing protocols (various flow rates, concentrations, catalyst loadings and spatial organizations, lamps and corresponding intensities,…), resulting in many different styles of reporting, making it very difficult to mutually compare results. In that regard several institutions are collaborating on the development of standardized photocatalytic test protocols.

Next to actual gaseous pollutants, PCO of organic solids can be considered as a border case of gas phase photocatalysis, as the reactions take place at the solid-gas interface, for instance after deposition of suspended solids in aerosols. Furthermore, the mass transfer laws governing the supply of O_2 or the carry-off of CO_2 are similar to those of gas phase reactions. Such reactions include PCO of polymer films such as polyethylene[56] and polystyrene[57], but also solid acids. The degradation of stearic acid films is a typical example of the latter. Stearic acid is considered as a good model compound for organic fouling on, for instance, glass windows and is therefore often the pollutant of choice for studies involving self-cleaning surfaces.[58–61] Recently, Mills and Krysa collaborated on the development of another quick qualitative test for evaluating photocatalytic performance based on color changes of solid resazurin ink films.[62] A final, socially relevant application of solid-gas heterogeneous PCO is the degradation of soot (black carbon) deposits. In this context Smits *et al.* have shown that it is possible to photocatalytically degrade considerable amounts of carbon black (ca. 22 µg cm^{-2}) using TiO_2-coated mortar substrates.[63] Within the framework of air pollution, the role of soot is becoming more and more prominent, which is why several groups' recent activities are concentrated on this emerging topic.[63–66]

3 FUNDAMENTALS OF PHOTOCATALYSIS

The previous sections underline the stringent need for air purification and illustrate that PCO could offer a viable solution. In first instance this chapter briefly reviews the fundamentals of photocatalytic reactions and points out the benefits and limitations. The second section of this chapter investigates the driving properties of gas phase photocatalysis in particular. Although this review focuses on 'classic' TiO_2-based photocatalysis, it has to be highlighted that in recent years a lot of work has been devoted to the development of alternative photocatalysts, other than TiO_2. These are often semiconductors based on d^0 transition metal cations such as Ta^{5+} and Nb^{5+}, or nitrides and oxides of Ga^{3+}, In^{3+} and Bi^{3+} (d^{10} configuration). Metal-organic frameworks (MOFs) make up another special class of alternative photocatalysts. Photoactivity has been demonstrated for several members of this material class such as MOF-5, UiO-66 and UiO-66(NH_2).[67–69] Hernández-Alonso *et al.* have reviewed a great number of these alternative catalyst materials, so we refer the interested reader to this review paper for more information.[70] The rest of this literature overview is restricted to TiO_2-based photocatalysts.

3.1 GENERALITIES OF TiO_2 PHOTOCATALYSIS

Anatase, rutile, brookite and TiO_2 (B) monoclinic are the four TiO_2 polymorphs that are encountered in nature, of which anatase is the most photoactive phase and rutile thermodynamically the most stable.[71] Both the anatase and rutile crystal lattices are composed of chains of TiO_6 octahedra, but with different connectivity. In the anatase lattice the octahedra share four edges (Figure 3a), whereas in rutile only two edges connect the octahedra with their nearest neighbors (Figure 3b). According to Pauling's third rule, structures tend to become less stable as the constituting polyhedra are connected by an increasing number of edges or faces due to increasing repulsion of the cationic cores. This explains why rutile is thermodynamically more stable than anatase.

As any semiconductor, TiO_2 is characterized by a band structure in which the energy levels of the valence band (highest occupied level) and conduction band (lowest unoccupied level) are separated by a band gap (E_g) of ca. 3.2 eV in the case of anatase.[72] A photocatalytic event is initiated when the catalyst is activated by light with an energy content that is sufficient to overcome the band gap.[73] The incident light wavelength is related to its energy content according to (eq. 1).

$$E = h\nu = \frac{hc}{\lambda} \qquad \text{(eq. 1)}$$

with E = energy content

h = Planck's constant (6.63×10^{-34} J s)

ν = frequency of incident light

c = speed of light (3×10^{8} m s^{-1})

λ = incident light wavelength

In the case of TiO_2 anatase the band gap energy corresponds to UV light with a wavelength of 388 nm or shorter to bridge the band gap. This enlightens one of the biggest limitations of TiO_2 photocatalysis, as UV light only contributes to ca. 5% of the entire solar spectrum. It would therefore be of tremendous interest to extend the photocatalytic activity towards the visible light region (400-700 nm) that contributes to an approximate additional 40% of the spectrum.[74]

After absorbing light of sufficient energy, an electron (e^-) is promoted from the valence band to the conduction band, leaving behind a positively charged hole (h^+) ((eq. 2) and Figure 4)

$$TiO_2 + h\nu \rightarrow e^-_{CB} + h^+_{VB} \qquad \text{(eq. 2)}$$

The photogenerated charge carriers can in turn initiate the reduction/oxidation of species adsorbed on the catalyst surface, depending on the relative positions of their redox potentials. At neutral pH, the redox potential of the hole on TiO_2 is +2.53 V, whereas that of the excited electron is -0.52 V (both

versus standard hydrogen electrode (SHE)).[75] Hence, reductions can only occur when the redox potential of the e^- is negative enough to reduce the oxidant, while oxidations only take place when the redox potential of the h^+ is more positive than that of the reductant. As an illustration, consider the application of H_2 gas evolution from H_2O (i.e. water splitting) (Figure 4). Two half reactions need to take place: reduction of H_2O to H_2 (-0.413 V vs. SHE) on the one hand and the oxidation of H_2O to O_2 (+0.83 V vs. SHE) on the other hand. Using UV-activated TiO_2, this reaction is allowed since the photogenerated electrons and holes are strong enough reducing agents (-0.52 V < -0.413 V) and oxidizing agents (2.53 V > 0.83 V), respectively.

With regard to the degradation of organic contaminants, the generally accepted reaction mechanism involves a radical pathway. The radical chain reaction is typically initiated by the formation of hydroxyl radicals ($^{\bullet}OH$) from H_2O (+2.27 V vs. SHE) and superoxide anion radicals ($O^{2-\bullet}$) from O_2 (-0.28 V vs. SHE) with the aid of photogenerated h^+ and e^-, respectively (equations (eq. 3) and (eq. 4)).[75,76] This is justified in view of the relative positions of the redox potentials (Figure 4). Subsequent reactions of $O^{2-\bullet}$ with H^+ can yield other reactive oxygen species such as hydroperoxyl radicals ($^{\bullet}OOH$), H_2O_2 and finally $^{\bullet}OH$ (eq. 5-7) that may participate in the further photocatalytic process.[71,74]

Singlet oxygen ($^1O_2$) is another specific oxygen species that can be formed through photo-oxidation of $O_2^{-\bullet}$ on the TiO_2 surface, often in sensitized reactions.[77–80] Direct oxidation of adsorbed organic species by photogenerated holes has also been reported, especially at low water content or high surface coverage of pollutant.[71,75,81]

$$H_2O + h_{VB}^+ \rightarrow {}^{\bullet}OH + H^+ \qquad \text{(eq. 3)}$$

$$O_2 + e_{CB}^- \rightarrow O_2^{-\bullet} \qquad \text{(eq. 4)}$$

$$O_2^{-\bullet} + H^+ \rightarrow {}^{\bullet}OOH \qquad \text{(eq. 5)}$$

$$^{\bullet}OOH + {}^{\bullet}OOH \rightarrow H_2O_2 + O_2 \qquad \text{(eq. 6)}$$

$$H_2O_2 + e_{CB}^- \rightarrow {}^{\bullet}OH + OH^- \qquad \text{(eq. 7)}$$

Apart from initiating a radical chain reaction, the possibility also exists for photogenerated charge carriers to neutralize one another (eq. 8). This process is known as recombination.[82,83] It is facilitated by lattice defects, crystal imperfections and impurities.[84] According to Hoffmann *et al.*,[85] charge recombination is a semi-fast process occurring on a time scale of 10-100 ns, whereas the initial charge generation is very fast (fs time scale) and interfacial charge transfer is rather slow (100 ns - ms time scale). Of course, recombination should be avoided as much as possible because it results in drastic efficiency decrease. Several strategies have been -and are being- considered in order

to reduce charge recombination by improving separation of e^--h^+ pairs (cfr. Section 5), thus enhancing the photocatalytic efficiency.

$$e_{CB}^- + h_{VB}^+ \rightarrow energy \qquad \text{(eq. 8)}$$

3.2 DRIVING PHOTOCATALYTIC PROPERTIES IN GAS PHASE

After these general considerations, it is useful to try defining the driving parameters of gas phase photocatalysis and how they differ from liquid phase PCO. An insightful case-study is offered by comparing the often used P25 (Evonik) and PC500 (Crystal Global) TiO_2-based photocatalysts.[41] In liquid phase PCO, P25 outperforms PC500.[86–89] In the gas phase PCO of acetaldehyde, however, the extreme opposite is observed.[41,90] Apparently, both catalysts possess characteristics that render them particularly more (un)suited for either gas or liquid phase applications. For more insight, an overview of the relative magnitude of several important photocatalytic and material properties of PC500 with respect to P25 is given in Table 2. From this table it is clear that the superior activity of PC500 in the gas phase PCO of acetaldehyde can be attributed to its larger specific surface area, absolute amount of surface OH-groups and adsorption capacity. However, considering adsorption properties alone, the turnover frequency (TOF) on PC500 should exceed the TOF on P25 by a factor of at least three. This is plainly not the case (factor 1.3), which is attributed to the unfavorable bulk properties of PC500, as evidenced by the low photocurrent ratio (<0.01). This is indicative of a lower photon utilization efficiency of the PC500 photocatalyst. It has to be added that in aqueous phase the low performance of the PC500 catalysts is in part expected to be due to adsorbed and bulk water in the small, intricate pore system (mean size around 4-5 nm) that will imply a serious mass transfer resistance. In addition, the pH of the solution in liquid phase PCO also plays an important role in governing the attraction/repulsion between the contaminants and the catalyst surface.[85]

Summarizing, good morphological properties can dominate the photocatalytic efficiency over poor electronic properties and is thus the main driving force for gas phase PCO. It is in fact useful to exploit the low mass transfer resistance encountered when working in gas phase by developing photoactive materials with high surface area, which in most cases will be quite accessible. On the other hand, the ideal gas phase photocatalyst should not only possess a large specific surface area and adsorption capacity, but also a high photon utilization efficiency. This implies that (i) light has to be able to penetrate the material and (ii) the incident photons should be absorbed and effectively induce the generation of free charge carriers. This means that two main issues should be addressed: the limited activity window of TiO_2 (restricted to UV light) and the tendency for free charge carriers to recombine. At this point it is evident that both morphological design (to the first degree) as well as electronic

modifications (to a second extent) can add substantially to the overall photocatalytic performance in gas phase. These two main types of photocatalyst modification will be the subject of the next two chapters.

4 MORPHOLOGICAL TiO_2 DESIGN AND SELECTED GAS PHASE EXAMPLES

As already indicated above, TiO_2 photocatalysis can benefit from morphological design in several ways. Nakata and Fujishima have proposed a classification of TiO_2 photocatalysts in four categories, based on their dimensionality (Figure 5).[91] In the following discussion this classification will be followed and extended with additional examples on gas phase applications. It is not the intention to discuss into detail all different synthesis strategies. The main goal is to give an overview of available TiO_2 catalyst architectures with the associated benefits and drawbacks and illustrate them with gas phase PCO studies. For an in-depth overview on photocatalyst design with more detail on synthesis procedures, the reader is referred to the excellent review article by Nakata and Fujishima.[91] Note that some structural modifications will also affect the electronic properties and vice versa.

4.1 NANOPARTICLES

As photocatalytic reactions take place at active sites on the TiO_2 surface, it is useful to maximize exposure of the catalyst surface to the gaseous environment and the light source.[41] By reducing the primary particle size, a very high surface-to-volume ratio can be obtained. A second advantage of using nanoparticles is offered by the short charge carrier diffusion distances involved, reducing e^--h^+ recombination.[92] By decreasing the particle size, an overall increase of photocatalytic performance has been shown for gas phase PCO of toluene,[93] ethanol and acetaldehyde,[94] amongst others. Also industrially, fabrication of photocatalyst powders with small particle sizes is a well-known strategy. For instance, Evonik's P25 Aeroxide, which is one of the most widely used commercial photocatalysts and the benchmark for most comparative studies, is a nano-sized powder with an average primary particle size of approximately 21 nm. Maira *et al.* demonstrated that 7 nm is the optimal size of TiO_2 nanoparticles for PCO of gaseous trichloroethylene.[39] Larger individual particles are deemed to be less efficient because less of the incident light is absorbed due to the larger scattered fraction, but this can be circumvented by the ultimate catalyst and/or reactor design. Multiple scattering can eventually lead to improved light utilization and associated high efficiencies.[34] On the other hand the activity also drops when decreasing the nanoparticle size below 7 nm. This is due to the fact that the TiO_2 semiconductor displays discretization of its band structure for such small particles. As a consequence, the band gap experiences a blue shift, leading to less efficient utilization of incoming photons.[95,96]

This phenomenon is better known as the "quantum size effect", that limits the exploitation of the net effect of increasing surface area by shrinking the particle size.

Fabrication of hollow nanospheres[97] or sphere-in-sphere structures[98] are more advanced variations on the theme of nanoparticle design. Such architectures show the additional advantage of multiple reflections of incident light inside the particles, leading to improved photon utilization.

4.2 NANOTUBES AND (HOLLOW) FIBERS

TiO_2 nanotubes (Figure 6a), nanofibers (Figure 6b), nanowires and other related one-dimensional structures possess similar advantages to zero dimensional nanoparticles.[99–101] They too benefit from high surface-to-volume ratios, as well as fast interfacial charge transfer, leading to low recombination rates, especially in the case of thin-walled hollow structures.[91] Furthermore, an assembly of fibrous or wire-like structures can serve as a mat that is well suited for practical gas phase applications such as gas sensing.[102,103] Creating additional surface area through the introduction of (multiple) hollow channels (Figure 6c) further enhances the photocatalytic activity of TiO_2 fibers. Gas phase PCO of acetaldehyde was shown to progress more efficiently, as the number of channels in hollow fibers increases. This result was attributed to a combined effect of better molecule trapping, as well as the occurrence of multiple light reflections in the cavities.[104] A similar effect was observed for long nanotube arrays that were also used in the PCO of acetaldehyde.[105]

4.3 NANOSHEETS AND THIN FILMS

TiO_2 nanosheets are commonly employed in applications involving self-cleaning surfaces, i.e. photocatalytic reactions at the solid-gas (or solid-liquid) interface. This is because of their specific properties. Nanosheets are flake-shaped structures with a thickness of a few nanometers and cross-sectional dimensions up to a few microns.[106] Generally, nanosheets adhere well onto various substrates and their surface is very smooth. That property is advantageous towards anti-fouling applications as it is more difficult for pollutants to stick to a smooth surface compared to rough surfaces. Thin, long and narrow belt-like structures can be considered as a special kind of nanosheets, called nanoribbons.[107,108]

TiO_2 thin films can be regarded to cross the bridge between two dimensional and three dimensional architectures. Very thin films (with a thickness of a few nanometers) can still be approximated as two dimensional. These films often consist of hard TiO_2 glazes prepared by various techniques, including vapor-type depositions (including atomic layer deposition, ALD),[61,109,110] sputtering,[111] sol-gel coating[112,113] and thermal methods.[114] A commercially available material that fits this category and is often used in comparative tests with self-cleaning surfaces, is Pilkington Activ™ glass,[115]

consisting of a 15 nm thick nanocrystalline TiO_2 layer.[116] Thicker films (sub-micron to several hundreds of microns) are usually prepared with the intention of introducing a certain degree of porosity or structural ordering. These can no longer be regarded as being two dimensional and will therefore be dealt with in the next section.

4.4 POROUS, INTERCONNECTED AND SUPPORTED STRUCTURES

Although quite some benefits are associated with the use of nanoparticles, a big disadvantage is that they have high tendency to agglomerate into larger aggregates. Generally this is at the expense of photocatalytic activity, but in particular cases it can also lead to an improved efficiency. Bahnemann's group have proposed the 'antenna mechanism', which involves the transfer of photon energy from one nanoparticle to another when they are arranged as an interconnected network along a fixed crystallographic orientation.[117] This could be an important effect in many TiO_2 powders consisting of large secondary agglomerates of closely interconnected crystalline nanoparticles. In many other cases, however, TiO_2 nanoparticles are incorporated into (porous) substrates or alternatively, (ordered) interconnected 3D structures of pure TiO_2 are synthesized.

4.4.1 TiO_2 supported on porous materials

Aggregation of individual nanoparticles is often prevented by their incorporation into porous substrates such as zeolites and (ordered) mesoporous silica.[118–120] Zeolites are micro- and mesoporous materials with uniform pore sizes and very good adsorption properties, which makes them interesting supports for environmental remediation when combined with TiO_2.[121–123] Gas phase PCO over TiO_2-zeolite composites has for instance been applied for the degradation of acetaldehyde,[124] pyridine[125] and propionaldehyde.[126] Another peculiar 3D support is of biological origin. Van Eynde *et al.* have used the silica frustule of diatoms (i.e. siliceous algae skeletons) as porous substrates with a multimodal pore size distribution for the fixation of TiO_2 in photocatalytic air purification applications (Figure 7a).[127,128] Apart from the selected examples mentioned above, many other ordered and unordered (bulk) (meso)porous supports are available and have been reviewed in literature.[120,129]

Next to accommodating or preventing agglomeration of nanoparticles, some supports can play an active role in the catalytic reaction. Especially carbonaceous supports often exert such a function, which has been thoroughly reviewed by Leary and Westwood.[130] For instance, TiO_2 can be deposited onto activated carbon. It is known that activated carbon is an excellent adsorbent. The combination with TiO_2 offers the very attractive feature that pollutants can be efficiently 'caught' from the surroundings and the reaction is less affected by excessive humidity levels. Thereafter they are photocatalytically degraded while surface concentrations are kept high.[131,132] Another example of

a carbonaceous substrate participating in the PCO reaction is the use of carbon nanotubes (CNTs). CNTs are well known for their excellent electron conductive properties. When TiO_2 is brought into electrochemical contact with CNTs, photogenerated electrons can be transported through the CNT from the spot of photo-excitation to the site where the reduction reactions take place. That way they are physically separated from the holes so the rate of charge carrier recombination is reduced. TiO_2-CNT composites have for instance proven to be quite efficient in the PCO of gaseous acetone and propene for this reason.[133,134] We have also exploited this effect for the swift electron transfer in a stand-alone photo-fuel cell that produces hydrogen gas from ambient humid air.[135] Alternatively, Faria's group has shown that CNTs may also act as sensitizers (cfr. Section 5.3.1) by generating e^--h^+-pairs on the tubes and subsequently transferring electrons to TiO_2.[136] Combination of TiO_2 with graphene (and fullerene) is also frequently encountered. The beneficial effect is again based on efficient conductivity of photogenerated electrons in order to reduce charge recombination, as shown for gas phase PCO of benzene.[137] Note that these are all examples of how design aspects simultaneously influence the electronic properties.

4.4.2 Porous and interconnected TiO_2 structures

It would be very convenient to have a strategy available that results in self-supporting, porous, macroscopic TiO_2 networks that can be readily incorporated in gas phase PCO reactors. A foam-like structure is a suitable candidate to this end because of its large exposed surface area and its open structure that keeps mass transfer resistances low and still allows sufficient light penetration. Keller's group made nice advancements in this domain by using foam-like supports for various gas phase applications, including disinfection of airborne bacteria.[139–141] An alternative strategy has been explored by Tytgat *et al.*, who fabricated self-supporting TiO_2 foams using a direct foaming technique (Figure 7b).[142] It was shown that these TiO_2 foams were active towards PCO of ethylene in the gas phase.

Usually a templating strategy is followed in order to fabricate structured TiO_2 networks. The sacrificial template technique involves deposition of TiO_2 onto, often ordered, foreign substrates. In the next step the foreign template is removed by chemical or thermal treatment, leaving an interconnected TiO_2 network with a structure commensurate to the original template. A high degree of porosity can be introduced due to pores and channels caused by the disappearance of the template. An illustration of this principle is given by some of our recent work in which carbon nanotubes and carbon nanosheets were used as sacrificial carbonaceous templates for atomic layer deposition (ALD) of TiO_2. A thin, conformal layer of TiO_2 was deposited on the surface of these carbonaceous structures. ALD was used as the deposition method since it ensures complete coverage of nanostructures with high aspect ratios, without obstructing the pores.[143] Calcination of the samples led to removal of the template,

crystallization into the photoactive anatase phase, and a morphology change into an interconnected network of TiO_2 nanoparticles with an overall morphology commensurate to the template (Figure 8). The obtained films thus present a very large surface area enhancement and were shown to be more active compared to commercially available reference materials in the gas phase PCO of acetaldehyde.[144–146]

A particular case of the templating method that deserves special attention is the synthesis of inverse opals as photonic structures.[147,148] Photonic structures are ordered materials with void sizes corresponding to the incident wavelength. Light that enters the crystal is trapped in those voids by multiple internal reflections and diffractions, increasing the effective optical path length through the catalyst (Figure 9).[149] This way the probability of light absorption and subsequent charge generation is enhanced. That is the reason why inverse opals are preferably designed to match light wavelengths corresponding to the onset of the semiconductor band gap, that normally have low probability of leading to e^--h^+-pair formation.[150] The study of Ren and Valsaraj on the use of TiO_2 inverse opals for the enhanced PCO of 1,2-dichlorobenzene is one of the few accounts in literature in which photonic structures are employed to improve gas phase photocatalysis.[151] This application again illustrates how morphologic engineering and electronic properties are intertwined.

5 MODIFYING TiO_2 ON THE ELECTRONIC LEVEL: PROMISING STRATEGIES AND SELECTED GAS PHASE EXAMPLES

A lot of effort has been devoted to improve the photo-electronic properties of TiO_2 in order to circumvent one of the two major limitations of TiO_2 photocatalysis:

(i) Tendency for photogenerated charge carriers to recombine

(ii) Photoactivity window restricted to UV illumination

In this section an overview is given on current strategies to bypass one or both of these shortcomings. The focus is laid on the most recent or promising developments.

5.1 DOPING

Semiconductor doping is the most encountered and facile way of changing the electronic properties of TiO_2 by altering the band gap. There are three main doping categories: self-doping, cation doping and anion doping. Co-doping with several elements simultaneously is a variation on the same theme.

5.1.1 Self-doping

The term "self-doping" refers to the fact that the TiO_2 semiconductor is changed without the introduction of other metals or non-metals. It is achieved by disrupting the stoichiometric oxygen

balance by generating vacancies in the lattice, giving rise to Ti^{3+} sites.[153] Oxygen vacancies are indeed known to be good e^- traps. These trapping states are located just below the conduction band. After visible light absorption they are promoted to the surface where they can participate in surface reactions, which has for instance been employed in the gas phase PCO of NO.[154,155] Mul's group reported the one-step synthesis of blue colored, Ti^{3+}-rich TiO_2 that is active under visible light illumination,[156] but such materials can suffer from stability issues. On the other hand, Pillai's group recently described the visible light activity of oxygen rich TiO_2. This was attributed to an upward shift of the valence band after thermal decomposition of peroxo-TiO_2 complexes.[157] The material remained stable up to 900°C due to an increased Ti-O-Ti bond strength.

5.1.2 Cation doping

Increasing visible light absorption through cation doping (with Fe, Cu, Mn, Mg, Al, Zn, Cr, Ag, Ni, Pb, Ca, etc.) has been the focus of many research efforts for more than two decades. Unfortunately, this strategy did not lead to big breakthroughs. Nonetheless there is a vast amount of literature available on the subject. It is impossible to strive for completeness within the limited frame of this literature overview. The interested reader is therefore referred to an extensive review by Litter on the effects of transition metal doping in photocatalysis and references therein.[158] The following discussion will thus be limited to general considerations and recent trends.

In general, the goal of cation doping is to introduce additional states in the TiO_2 band gap.[92] These impurity levels result in more absorption in the visible light region of the spectrum because energy transitions are enabled that require less energy (Figure 10). The resulting energy levels of the dopant states and resulting photocatalytic activity strongly depend on several factors: the chemical nature of the dopant, its concentration and its chemical and structural environment. It is obvious that every metal will exhibit a different effect on the activity and even for a given metal cation, the resulting effect may differ depending on the synthesis or reaction conditions.[159] With regard to dopant concentration, there is a consensus that at low amounts, the dopants act as trapping sites that can improve charge separation and introduce intermediate energy levels in the band gap that promote electron excitation at longer (visible light) wavelengths. At higher concentrations they can become recombination sites.[160] Hence, there often exists an optimum amount of dopant, which is typically in the order of 1 wt% or lower (TiO_2 basis). The influence of the structural environment of the dopant is illustrated by Sun *et al.*, who did not observe visible light activity when the cations were present as surface complexes.[161] The requirement for ion incorporation in the bulk lattice is also confirmed by Kang *et al*.[162] Metal ions that are not well incorporated in the lattice may block active sites at the surface and lead to lower activities.

One recent trend that emerged the last five to ten years is doping with metals from the lanthanide group of the periodic table. Especially doping with Ce is a promising approach. It has a high thermal stability, as well as adsorption selectivity that may improve adsorption of pollutants at the catalyst surface, as has been shown in the case of nitrite adsorption on 0.7wt%Ce-TiO_2.[163] Another special feature of Ce is that it acts as a good structural promoter. Ce doping leads to well-defined mesoporosity and an increased thermal stability of the anatase phase,[164] which is beneficial for gas phase applications that benefit strongly from increased surface area. Several researchers have observed a retardation in the crystal growth and a suppression of the thermal anatase to rutile recrystallization.[164,165] This structural stabilizing effect is attributed to the formation of Ti-O-Ce species at the surface, as a consequence of the large atomic radius that prevents Ce from being incorporated in the TiO_2 lattice.[159,163] A final aspect of Ce doping is the increased visible light absorption. The Ce^{3+}/Ce^{4+} redox potential (1.8 eV) lies within the TiO_2 band gap. Consequently, a red shift is observed in the range of 400-500 nm after doping with Ce.[166,167]

5.1.3 Anion Doping

Increasing visible light absorption by doping with anions has been considered since the end of the 1980's. Carbon, fluorine, sulfur, boron, phosphor and halides are all known examples, but doping with nitrogen has attracted most attention since the first discovery of Sato *et al.* in 1986.[168] It is easily incorporated in the TiO_2 lattice due to its low ionization potential and comparable atomic radius to oxygen.[169] On the other hand, the precise chemical nature and location of the species that account for the enhanced visible light absorption of N-doped TiO_2 is still under debate: NO_x, NH_x, N^{2-}, NO^-, NO_2^- and NO_3^- have all been proposed.[170] There is a general hypothesis that incorporation of anions with lower electronegativity than oxygen in the TiO_2 lattice, results in an upward shift of the 2p-levels of the valence band and thus narrows the band gap, in contrast to cation doping that results in additional energy states within the band gap itself (Figure 10). At this point it is not 100% clear whether the N-related states are localized or intrinsically part of the band gap.[84]

An interesting application of anion doping for air purification is demonstrated by Li *et al.*[171] They studied N-F-co-doped TiO_2 for the degradation of gaseous acetaldehyde, toluene and trichloroethylene in a simulated a commercial blue LED air cleaner. Co-doping of nitrogen and fluorine showed a synergetic effect. N-doping led to an increased visible light absorption, while F-doping led to the formation of new active sites through the introduction of oxygen vacancies that give rise to $^{\bullet}OH$ and $O_2^{-\bullet}$ radicals.

As a final remark, it is important to realize that although the main idea of ion doping is to increase visible light absorption, high visible light *absorption* does not necessarily mean high visible light photocatalytic *activity*!

5.2 COMPOSITE SEMICONDUCTORS

By bringing two independent semiconductors into close electrochemical contact, photogenerated charge carriers can be transferred from one component to the other. The result is an improved charge separation, less recombination, with expected higher photocatalytic activity. SnO_2/TiO_2 and WO_3/TiO_2 are two representative examples of such composites.[172–175] In both cases the TiO_2 conduction band position is more negative and the TiO_2 valence band position is less positive than the conduction and valence bands of the other oxide respectively. This enables a vectorial charge transfer after photo-excitation that results in a physical separation of electrons and holes (Figure 11).

Interestingly, this type of charge separation can also occur in polymorphic TiO_2 (i.e. co-presence of anatase and rutile). It has been suggested that the good photocatalytic performance of commercial P25 (Evonik) is not only attributable to its nanocrystalline nature, but also to its polymorphic composition (roughly 80% anatase, 20% rutile). After the initial work of Bickley *et al.*[177] and several other researchers trying to unravel the synergy of anatase and rutile,[178–181] Ohtani *et al.* concluded in 2010 that the different fractions of P25 behave independently, without any interaction.[182] However, one year later Su *et al.* contradicted this finding in a convincing study that demonstrates the synergetic effect for anatase-rutile composites with an anatase content of at least 40% and rutile fraction of at least 20%.[176] Their study was unique in that sense that different composite samples were prepared in which only the anatase/rutile ratio was altered. All other morphological parameters were kept constant. Since morphological parameters are ruled out of the equation, it can be expected that the synergy is an intrinsic catalytic property and thus applies to both liquid and gas phase reactions. A maximal synergetic effect was observed in their experiments for 60% anatase and 40% rutile, which was 50% higher compared to pure anatase (Figure 12). This result is confirmed by surface photovoltage measurements of TiO_2 nanopowders with variable rutile content by our group.[90]

5.3 SENSITIZED AND PLASMONIC TiO_2

This final part on modification of the electronic properties of TiO_2 deals with the use of nanostructures in contact with the TiO_2 surface in order to induce or enhance visible light activity. Two main categories are considered: sensitizers and nanoparticles displaying surface plasmon resonance.

5.3.1 Sensitizers

The general principle of a photosensitizer in electrochemical contact with a substrate (e.g. TiO_2) is that it absorbs visible light energy and transforms it into chemical energy that in turn can be transferred to the otherwise inactive oxide (Figure 13a).[183] Photosensitized photochemistry has mainly been employed in application fields such as dye-sensitized solar cells (DSSC) or Grätzel cells,[184] semiconductor-sensitized solar cells (SSSC),[185] water splitting[186,187] and water

purification.[188,189] In order to restore the sensitizer to its ground state, an electron donor (e.g. EDTA) is added to the solution.[190] This technical requirement is the main reason why photosensitization is not a common approach in gas phase photocatalysis, where sensitizer depletion is observed.[191]

Photosensitizers can be classified into three major categories: inorganic sensitizers (quantum dots), organic dyes, and organo-metal complexes. Inorganic sensitizers are in fact narrow band gap semiconductors such as CdS, CdSe, PbS and ZnS.[193–195] They have a more negative conduction band compared to TiO_2 thus enabling the transfer of visible photogenerated electrons from the narrow band gap semiconductor to TiO_2. A unique property of quantum dots is that, due to their nanometer size, they show quantum confinement effects that allow to tune their absorption spectrum by varying the particle size.[196] They also show high extinction coefficients, so a thin layer of quantum dots (Figure 13b) already leads to appreciable visible light absorption. Plenty of organic dyes have been employed as sensitizers. Examples include eosin Y,[191] rose bengal,[188] and cresyl violet.[197] The large drawback of dyes is their lack of stability. Dissolution as well as photocatalytic degradation of the dyes has been reported.[190] Finally, organo-metal complexes can also be applied as sensitizers. They often possess chromophoric centers that mimic nature's light harvesting systems. Known examples include Ru complexes,[198] Os porphyrines[199] and Pt complexes[200] anchored to the TiO_2 surface.

5.3.2 Plasmonic photocatalysis

Surface plasmon resonance (SPR) is a unique optical property of metallic nanoparticles that arises from a photo-induced collective oscillation of conduction band electrons.[201] SPR enables concentrating and manipulating light at the nanoscale. This led to a myriad of applications ranging from sensors,[202] over energy production,[203] biochemical applications,[204,205] surface enhanced Raman spectroscopy (SERS),[206,207] to environmental remediation through photocatalysis.[208,209] The interested reader is also encouraged to read the recent review paper by Zhang *et al.* that includes more photo-physical aspects of plasmonic photocatalysis, also on materials other than TiO_2.[210]

Although the use of SPR in nanotechnology seems a recent development, exploitation of the unique optical properties of noble metal nanoparticles dates back to thousands of years ago.[211,212] For instance, red glassware from the late Bronze era (1200-1000 BC) was colored by means of copper nanoparticles. The *Lycurgus* Cup from the 4^{th} century (AD) has the peculiar property that when the glass of the cup is illuminated, its color changes from yellowish-green to bright ruby-red, which is attributed to the presence of gold-silver alloy nanoparticles (Figure 14). A lot of the still existing stained glass frames in medieval churches receive their color from the presence of metallic nanoparticles displaying SPR. It is amazing that only in 1908, thanks to the work of Gustav Mie, people actually started to realize that they were practicing nanotechnology all along![213]

An important physical feature of plasmonic nanoparticles is their extinction cross section, equal to the sum of the absorption and scattering cross sections.[214] For particles much smaller than the incident light wavelength, the contribution of scattering is negligible and extinction is mainly determined by absorption.[214,215] Plasmonic nanoparticles can have absorption cross sections several times larger than their actual size.[216,217] Tuning of the SPR maximum to a specific wavelength is an important tool for achieving efficient utilization of incident light in various applications. Therefore the different factors that exert an influence on the SPR wavelength need to be taken into consideration. The first, quite obvious parameter that influences SPR, is the kind of metal that is used. The most encountered metals are those with pronounced SPR in the visible range of the spectrum, such as gold, silver and copper (Figure 15a). An alternative way of SPR wavelength tuning is the fabrication of metal alloy nanoparticles. This strategy enables to cover a wide range of SPR wavelengths by merely altering the alloy composition (Figure 16).[218] A second parameter that governs the SPR wavelength is particle size. Although a small red-shift of the SPR maximum occurs with increasing particle size, the dominant effects are broadening and increasing the intensity of the absorption band (Figure 15b).[217] A third influencing parameter is the shape of the particles. Not only spherical particles, but also a lot of other nanosized architectures such as rods,[219,220] cubes,[221] wires,[222] and many other (organized) geometries display SPR effects. Since the restoring force for the electron oscillation in plasmonic structures depends on the charge accumulation on the surface, it will be affected by the geometry. This is quite clear in the case of plasmonic nanorods. The charge accumulation, proportional to the restoring force, is small along the rod axis and bigger in the perpendicular direction. Therefore SPR occurs at larger wavelengths (lower energy) for oscillations along the rod axis (longitudinal plasmons) and at shorter wavelengths for oscillations along the radial direction (transversal plasmons). The larger the aspect ratio of the rod, the larger the red-shift of longitudinal plasmons. This is a general trend: the larger the deviation from sphericity, the more SPR shifts towards longer wavelengths.[220] A final main parameter affecting SPR is the dielectric environment. The charge accumulation at the particle surface induces an electric field in the near surrounding environment. This induces polarization of the medium which partially balances the charge accumulation at the surface, reducing the restoring force and consequently shifting SPR towards longer wavelengths.[216] The higher the dielectric constant of the medium (ε_m), the more pronounced this effect will be (Figure 15c).

The main concern within the context of this review is how these plasmonic structures can be used to improve photocatalytic performance under visible light illumination. In recent years, quite some studies have been published on the subject, mainly with regard to photocatalytic water splitting.[209,224,225] Despite all efforts, the exact mechanism of plasmon mediated photocatalysis is still under debate. A number of possible mechanisms have been proposed and tentatively proven, but

there seems to be no overall consensus, except for the fact that the highest activities on plasmonic photocatalysts are obtained when the incident light wavelength matches the SPR wavelength. Linic *et al.* describe the three prevailing explanations, that can be regarded as non-mutually exclusive mechanisms: (i) direct charge injection, (ii) near-field enhancement and (iii) extended optical path length by plasmon induced scattering (Figure 17).[226]

The direct charge injection mechanism is quite similar to the mechanism of photosensitization. Light absorption at the SPR wavelength leads to the formation of excited, energetic electrons. Under the right conditions and with intimate electrochemical contact between the plasmonic particle and the semiconductor, an electron is transferred from the excited plasmon state to the TiO_2 conduction band (Figure 17a). For instance, the studies by Silva *et al.*,[225] Tsukamoto *et al.*,[227] Tian and Tatsuma,[228,229] and Kowalska *et al.*[208] are all based on plasmon-induced charge transfer as the working hypothesis in relation to their observations.

The enhanced near-field hypothesis assumes radiative energy transfer between metal and semiconductor. The electrical field associated with charge accumulation on the metal surface can be quite intense. The field intensity drops exponentially with increasing distance from the nanoparticle, but it can still be significant at a distance of several nanometers (Figure 17b). Since the amount of e^--h^+ formation in a photocatalyst is proportional to the intensity of the surrounding electromagnetic field, it is to be expected that more photogenerated charge carriers are formed in the close vicinity of plasmonic nanoparticles. Because the field intensity strongly decreases with distance, more charge carriers are generated close to the semiconductor surface, rather than in the bulk.[226] Consequently short charge carrier diffusion distances apply that minimize charge recombination, and potentially lead to higher photocatalytic efficiency. Awazu and coworkers provided strong evidence for this near-field mechanism.[230] They covered plasmonic silver nanoparticles with layers of SiO_2 of increasing thickness to prevent direct contact with TiO_2. The photocatalytic activity decreased with increasing thickness of the SiO_2 barrier, which is in accordance with the proposed mechanism. Liu *et al.*,[224] Kumar *et al.*[231], Amrollahi *et al*.[232] and Christopher *et al.*[233] use this enhanced near-field mechanism to explain their findings. As a last point of attention, one should be aware that field enhancement can only be successful if the photocatalytic semiconductor already shows at least modest activity at the incident light wavelength used to generate SPR.[231,233] Indeed, the field *intensity* is increased by SPR, but not its *energy* level to overcome the band gap.

The final mechanistic hypothesis is mainly important for large plasmonic nanoparticles, i.e. with diameters of the same order of magnitude as the incident light wavelength. In contrast to small nanoparticles, light extinction for large nanoparticles is mainly due to scattering.[234] This property is

exploited in order to increase the effective optical path length of incident light inside the metal-semiconductor system, as illustrated in Figure 17c.

Apart from the three prevailing mechanisms discussed above, local heating of plasmonic nanoparticles and direct photocatalysis on plasmonic nanostructures have also been proposed.[235,236]

Although the current discussion on plasmonic photocatalysis is extensive, the number of actual applications with regard to TiO_2 photocatalysis in the gas phase are scarce to non-existent. With this we hope that this fascinating research domain will also prove its potential in photocatalytic environmental remediation. A first step in this direction is provided by our group by studying the degradation of stearic acid at the solid-gas interface. Gold-silver plasmonic alloy nanoparticles were used to tune the photocatalytic activity of TiO_2 to the solar spectrum.[223] Very recently it has been confirmed by means of action spectra and photocurrent measurements that such gold-silver alloy-TiO_2 photocatalysts can be used for solar-driven applications.[237]

As a final remark it is important to distinguish between visible light and UV illumination of metal-TiO_2 nanostructures. Under visible light illumination, the goal is to exploit the plasmon response on the metal in order to induce visible light photocatalytic activity of TiO_2. Under UV illumination on the other hand, TiO_2 is intrinsically able to generate charge carriers and the metals do not necessarily display SPR at the incoming wavelength. Still, in these conditions they can serve as co-catalysts that offer active sites with lowered activation barriers. Furthermore they can act as electron sinks, ensuring efficient e^--h^+ separation.[238–240]

6 TECHNO-ECONOMIC CONSIDERATIONS CONCERNING PHOTOCATALYTIC GAS PHASE APPLICATIONS

The success of a photocatalytic reaction is not solely determined by the catalyst properties, but also by reactor design and operating conditions. A key aspect to take into account in photoreactor development is the immobilization of the catalyst. Especially in gas phase applications involving high air flow rates, it is crucial to contain nanosized particles so they do not become airborne and pose a risk to human health. Process parameters such as light intensity, pollutant concentration, amount of catalyst present, flow rate and temperature obviously all affect the PCO efficiency.[241,242] Another very important parameter is gas humidity. It is commonly observed that PCO is impeded in the absence of water vapor.[42,243] On the other hand, an excess of water vapor can also inhibit PCO because water molecules competitively adsorb on the active sites.[244] Another important process condition is the composition of the gas feed. Sometimes the presence of certain VOCs can cause cross-sensitivity of PCO for other VOCs.[245] Conversely, when partial degradation of certain compounds yields radicals

with a high oxidation potential (e.g. •Cl), the rate of PCO might be enhanced for other pollutants present.[243,246]. From all this it is clear that careful control over all different process parameters is crucial in photocatalytic research and applications, but this is outside the scope of this overview.

From a socio-economic perspective, photocatalytic air purification still offers great opportunities. Already 15 years ago, Fisk estimated that the productivity gains that may be obtained by improving indoor air quality in the United States amount to 6-14 billion USD by reducing respiratory diseases, 1-4 billion USD by reducing allergies and asthma, 10-30 billion USD from decreased Sick Building Syndrome (SBS) symptoms and 20-160 billion USD dollars by improving general worker performance.[247] In that regard it is surprising that a BCC Research market survey from 2010 reported that only 0.5% of the total photocatalyst product sector is directly related to environmental applications. The largest share (87.4%) is accounted for by the construction sector (photocatalysts in building materials).[248] It has to be noted that the latter can also indirectly exert a beneficial influence on the environment, mainly through passive systems (e.g. coated surfaces exposed to the surrounding environment). Given these appealing prospects and the ample room for growth in the photocatalyst sector for environmental applications, it is wise not only to focus on improving the performance of photocatalysts through all kinds of high-end modification methods, but also keep taking into account the resulting costs, especially with the eye on commercialization.[249]

7 GENERAL CONCLUSIONS AND OUTLOOK

Photocatalysis has proven to be a viable technology for environmental air remediation. Its use has been demonstrated towards the abatement of various simple and complex, common and less encountered pollutants from indoor as well as outdoor sources. One particular compound that has not received much attention so far, is (airborne) particulate matter (consisting of soot and other poly aromatic organic and inorganic components). Employing photocatalysis in order to reduce soot concentrations in air could be a promising new area of application.

With regard to catalyst modification a lot has been achieved over the last years. The synthesis and use of nanoparticles has been studied quite extensively. Nanotubes, interconnected structures and (ordered) porous materials remain attractive building blocks for new and improved photocatalysts. The number of possible architectures that can be created is endless. In combination with properly conceived reactor design, this could mean a big step forward in photocatalytic efficiency. Photoreactor design could benefit a lot from accurate models, for instance based on computational fluid dynamic

calculations, that take into account the entire photocatalytic process (flow pattern, mass transfer,...) and not only overall reaction kinetics.[250]

Tuning of electronic properties of TiO_2 photocatalysts has evolved a lot over the past few decades. Improving charge separation through formation of composite structures is a very efficient approach. Inducing visible light activity by cation doping seems to become less popular and many alternative approaches have been proposed. Particularly (dye) sensitized and plasmon-mediated visible light active photocatalysis have recently become hot research topics. Applications of these materials in the field of air purification are, however, extremely scarce, which opens up a whole new world of opportunities.

ACKNOWLEDGEMENTS

The author wishes to thank the Research Foundation Flanders (FWO) for the financial support and postdoctoral fellowship.

REFERENCES

[1] World Health Organization, Global health observatory map gallery, data 2008, (2011). http://gamapserver.who.int/mapLibrary/.
[2] European Environment Agency, Cristina Guerreiro, Frank de Leeuw, Valentin Foltescu, Air quality in Europe - 2012 report.
[3] U.S.E.P. Agency, Residential air cleaners (second edition): a summary of available information, 2009.
[4] S.S. Kim, D.H. Kang, D.H. Choi, M.S. Yeo, K.W. Kim, Comparison of strategies to improve indoor air quality at the pre-occupancy stage in new apartment buildings, Build. Environ. 43 (2008) 320–328.
[5] Y.H. Chu, H.J. Kim, K.Y. Song, Y.G. Shul, K.T. Jung, K. Lee, et al., Preparation of mesoporous silica fiber matrix for VOC removal, Catal. Today. 74 (2002) 249–256.
[6] R. Andreozzi, V. Caprio, A. Insola, R. Marotta, Advanced oxidation processes (AOP) for water purification and recovery, Catal. Today. 53 (1999) 51–59.
[7] M.F. Boeniger, Use of ozone generating devices to improve indoor air-quality, Am. Ind. Hyg. Assoc. J. 56 (1995) 590–598.
[8] G.R. Peyton, W.H. Glaze, Destruction of pollutants in water with ozone in combination with ultraviolet-radiation. 3. Photolysis of aqueous ozone, Environ. Sci. Technol. 22 (1988) 761–767.
[9] N. Djeghri, M. Formenti, F. Juillet, S.J. Teichner, Photointeraction on surface of titanium-dioxide between oxygen and alkanes, Faraday Discuss. 58 (1974) 185–193.
[10] R.I. Bickley, G. Munuera, F.S. Stone, Photoadsorption and photocatalysis at rutile surfaces. 2. Photocatalytic oxidation of isopropanol, J. Catal. 31 (1973) 398–407.
[11] R.I. Bickley, F.S. Stone, Photoadsorption and photocatalysis at rutile surfaces. 1. Photoadsorption of oxygen, J. Catal. 31 (1973) 389–397.
[12] A. Mills, S. Le Hunte, An overview of semiconductor photocatalysis, J. Photochem. Photobiol. A. 108 (1997) 1–35.

[13] A. Mills, R.H. Davies, D. Worsley, Water-purification by semiconductor photocatalysis, Chem. Soc. Rev. 22 (1993) 417–425.
[14] J.M. Herrmann, Heterogeneous photocatalysis: fundamentals and applications to the removal of various types of aqueous pollutants, Catal. Today. 53 (1999) 115–129.
[15] A.G. Rincón, C. Pulgarin, Use of coaxial photocatalytic reactor (CAPHORE) in the TiO_2 photo-assisted treatment of mixed E. coli and Bacillus sp. and bacterial community present in wastewater, Catal. Today. 101 (2005) 331–344.
[16] M. Ni, M.K.H. Leung, D.Y.C. Leung, K. Sumathy, A review and recent developments in photocatalytic water-splitting using TiO_2 for hydrogen production, Renew. Sustain. Energy Rev. 11 (2007) 401–425.
[17] X.B. Chen, S.H. Shen, L.J. Guo, S.S. Mao, Semiconductor-based photocatalytic hydrogen generation, Chem. Rev. 110 (2010) 6503–6570.
[18] A. Hakki, R. Dillert, D. Bahnemann, Photocatalytic conversion of nitroaromatic compounds in the presence of TiO_2, Catal. Today. 144 (2009) 154–159.
[19] A. Hakki, R. Dillert, D.W. Bahnemann, Factors affecting the selectivity of the photocatalytic conversion of nitroaromatic compounds over TiO_2 to valuable nitrogen-containing organic compounds, Phys. Chem. Chem. Phys. 15 (2013) 2992–3002.
[20] K.H. Park, H.S. Joo, K. Il Ahn, K. Jun, One step synthesis of 4-ethoxy-1,2,3,4-tetrahydroquinoline from nitroarene and ethanol: A TiO_2 mediated photocatalytic reaction, Tetrahedron Lett. 36 (1995) 5943–5946.
[21] A. Apter, A. Bracker, M. Hodgson, J. Sidman, W.Y. Leung, Epidemiology of the sick building syndrome, J. Allergy Clin. Immunol. 94 (1994) 277–288.
[22] S. Devahasdin, C. Fan, K. Li, D.H. Chen, TiO_2 photocatalytic oxidation of nitric oxide: transient behavior and reaction kinetics, J. Photochem. Photobiol. A. 156 (2003) 161–170.
[23] F.B. Li, X.Z. Li, C.H. Ao, M.F. Hou, S.C. Lee, Photocatalytic conversion of NO using TiO_2-NH_3 catalysts in ambient air environment, Appl. Catal. B. 54 (2004) 275–283.
[24] B. Hauchecorne, T. Tytgat, D. Terrens, F. Vanpachtenbeke, S. Lenaerts, Validation of a newly developed FTIR in situ reactor: Real time study of photocatalytic degradation of nitric oxide, Infrared Phys. Technol. 53 (2010) 469–473.
[25] J.S. Dalton, P.A. Janes, N.G. Jones, J.A. Nicholson, K.R. Hallam, G.C. Allen, Photocatalytic oxidation of NO_x gases using TiO_2: a surface spectroscopic approach, Environ. Pollut. 120 (2002) 415–422.
[26] B.N. Shelimov, N.N. Tolkachev, O.P. Tkachenko, G.N. Baeva, K. V Klementiev, A.Y. Stakheev, et al., Enhancement effect of TiO_2 dispersion over alumina on the photocatalytic removal of NO_x admixtures from O_2-N_2 flow, J. Photochem. Photobiol. A. 195 (2008) 81–88.
[27] M. Hassan, L.N. Mohammad, S. Asadi, H. Dylla, S. Cooper, Sustainable photocatalytic asphalt pavements for mitigation of nitrogen oxide and sulfur dioxide vehicle emissions, J. Mater. Civ. Eng. 25 (2013) 365–371.
[28] Y. Zhao, J. Han, Y. Shao, Y. Feng, Simultaneous SO_2 and NO removal from flue gas based on TiO_2 photocatalytic oxidation, Environ. Technol. 30 (2009) 1555–1563.
[29] R.M. Alberici, W.F. Jardim, Photocatalytic destruction of VOCs in the gas-phase using titanium dioxide, Appl. Catal. B. 14 (1997) 55–68.
[30] H. Einaga, S. Futamura, T. Ibusuki, Heterogeneous photocatalytic oxidation of benzene, toluene, cyclohexene and cyclohexane in humidified air: comparison of decomposition behavior on photoirradiated TiO_2 catalyst, Appl. Catal. B. 38 (2002) 215–225.
[31] W.C. Hung, S.H. Fu, J.J. Tseng, H. Chu, T.H. Ko, Study on photocatalytic degradation of gaseous dichloromethane using pure and iron ion-doped TiO_2 prepared by the sol-gel method, Chemosphere. 66 (2007) 2142–2151.
[32] S. Yamazaki, A. Yoshida, H. Abe, Photocatalytic degradation of chloroform in the gas phase on the porous TiO_2 pellets: effect of Cl accumulated on the catalyst surface, J. Photochem. Photobiol. A. 169 (2005) 191–196.

[33] T. Tytgat, B. Hauchecorne, A.M. Abakumov, M. Smits, S.W. Verbruggen, S. Lenaerts, Photocatalytic process optimisation for ethylene oxidation, Chem. Eng. J. 209 (2012) 494–500.
[34] S.W. Verbruggen, S. Ribbens, T. Tytgat, B. Hauchecorne, M. Smits, V. Meynen, et al., The benefit of glass bead supports for efficient gas phase photocatalysis: Case study of a commercial and a synthesised photocatalyst, Chem. Eng. J. 174 (2011) 318–325.
[35] N. Bouazza, M.A. Lillo-Ródenas, A. Linares-Solano, Enhancement of the photocatalytic activity of pelletized TiO_2 for the oxidation of propene at low concentration, Appl. Catal. B. 77 (2008) 284–293.
[36] L. Cao, A. Huang, F.J. Spiess, S.L. Suib, Gas-phase oxidation of 1-Butene using nanoscale TiO_2 photocatalysts, J. Catal. 188 (1999) 48–57.
[37] T.N. Obee, R.T. Brown, TiO_2 photocatalysis for indoor air applications - effects of humidity and trace contaminant levels on the oxidation rates of formaldehyde, toluene, and 1,3-Butadiene, Environ. Sci. Technol. 29 (1995) 1223–1231.
[38] S. Ozaki, L.H. Zhao, T. Amemiya, K. Itoh, M. Murabayashi, Gas-phase photocatalytic degradation of cis-1,2-dichloroethylene using titanium dioxide under near-UV-illumination, Appl. Catal. B. 52 (2004) 81–89.
[39] A.J. Maira, K.L. Yeung, C.Y. Lee, P.L. Yue, C.K. Chan, Size effects in gas-phase photo-oxidation of trichloroethylene using nanometer-sized TiO_2 catalysts, J. Catal. 192 (2000) 185–196.
[40] S. Hager, R. Bauer, G. Kudielka, Photocatalytic oxidation of gaseous chlorinated organics over titanium dioxide, Chemosphere. 41 (2000) 1219–1225.
[41] S.W. Verbruggen, K. Masschaele, E. Moortgat, T.E. Korany, B. Hauchecorne, J.A. Martens, et al., Factors driving the activity of commercial titanium dioxide powders towards gas phase photocatalytic oxidation of acetaldehyde, Catal. Sci. Technol. 2 (2012) 2311–2318.
[42] J. Peral, D.F. Ollis, Heterogeneous photocatalytic oxidation of gas-phase organics for air purification: Acetone, 1-butanol, butyraldehyde, formaldehyde, and m-xylene oxidation, J. Catal. 136 (1992) 554–565.
[43] S.B. Kim, H.T. Jang, S.C. Hong, Photocatalytic degradation of gas-phase methanol and toluene using thin-film TiO_2 photocatalyst 1. Influence of water vapor, molecular oxygen and temperature, J. Ind. Eng. Chem. 8 (2002) 156-161.
[44] J.M. Coronado, S. Kataoka, I. Tejedor-Tejedor, M.A. Anderson, Dynamic phenomena during the photocatalytic oxidation of ethanol and acetone over nanocrystalline TiO_2: simultaneous FTIR analysis of gas and surface species, J. Catal. 219 (2003) 219–230.
[45] D. Vildozo, C. Ferronato, M. Sleiman, J.M. Chovelon, Photocatalytic treatment of indoor air: Optimization of 2-propanol removal using a response surface methodology (RSM), Appl. Catal. B. 94 (2010) 303–310.
[46] J. Kirchnerova, M.L. Herrera Cohen, C. Guy, D. Klvana, Photocatalytic oxidation of n-butanol under fluorescent visible light lamp over commercial TiO_2 (Hombicat UV100 and Degussa P25), Appl. Catal. A. 282 (2005) 321–332.
[47] J.M. Coronado, M.E. Zorn, I. Tejedor-Tejedor, M.A. Anderson, Photocatalytic oxidation of ketones in the gas phase over TiO_2 thin films: a kinetic study on the influence of water vapor, Appl. Catal. B. 43 (2003) 329–344.
[48] W.A. Jacoby, D.M. Blake, J.A. Fennell, J.E. Boulter, L.M. Vargo, M.C. George, S.K. Dolberg, Heterogeneous photocatalysis for control of volatile organic compounds in indoor air, J. Air Waste Manage. Assoc. 46 (1996) 891–898.
[49] N. Bouazza, M.A. Lillo-Ródenas, A. Linares-Solano, Photocatalytic activity of TiO_2-based materials for the oxidation of propene and benzene at low concentration in presence of humidity, Appl. Catal. B. 84 (2008) 691–698.
[50] M. Keshmiri, T. Troczynski, M. Mohseni, Oxidation of gas phase trichloroethylene and toluene using composite sol-gel TiO_2 photocatalytic coatings, J. Hazard. Mater. 128 (2006) 130–137.
[51] A. Bouzaza, A. Laplanche, Photocatalytic degradation of toluene in the gas phase: comparative study of some TiO_2 supports, J. Photochem. Photobiol. A. 150 (2002) 207–212.

[52] L. Palmisano, M. Schiavello, A. Sclafani, G. Martra, E. Borello, S. Coluccia, Photocatalytic oxidation of phenol on TiO_2 Powders - A Fourier-transform infrared study, Appl. Catal. B. 3 (1994) 117–132.
[53] S.Y. Lu, Q.L. Wang, A.G. Buekens, J.H. Yan, X.D. Li, K.F. Cen, Photocatalytic decomposition of gaseous 1,2-dichlorobenzene on TiO_2 films: Effect of ozone addition, Chem. Eng. J. 195-196 (2012) 233–240.
[54] C.H. Wu, G.P. Chang-Chien, W.S. Lee, Photodegradation of tetra- and hexachlorodibenzo-p-dioxins, J. Hazard. Mater. 120 (2005) 257–263.
[55] C.H. Wu, G.P. Chang-Chien, W.S. Lee, Photodegradation of polychlorinated dibenzo-p-dioxins: comparison of photocatalysts, J. Hazard. Mater. 114 (2004) 191–197.
[56] X. Zhao, Z. Li, Y. Chen, L. Shi, Y. Zhu, Solid-phase photocatalytic degradation of polyethylene plastic under UV and solar light irradiation, J. Mol. Catal. A. 268 (2007) 101–106.
[57] T. Tatsuma, S. Tachibana, A. Fujishima, Remote oxidation of organic compounds by UV-irradiated TiO_2 via the gas phase, J. Phys. Chem. B. 105 (2001) 6987–6992.
[58] A. Mills, N. Elliott, I.P. Parkin, S.A. O'Neill, R.J.H. Clark, Novel TiO_2 CVD films for semiconductor photocatalysis, J. Photochem. Photobiol. A. 151 (2002) 171–179.
[59] A. Mills, J.S. Wang, Simultaneous monitoring of the destruction of stearic acid and generation of carbon dioxide by self-cleaning semiconductor photocatalytic films, J. Photochem. Photobiol. A. 182 (2006) 181–186.
[60] Y. Paz, Z. Luo, L. Rabenberg, A. Heller, Photooxidative self-cleaning transparent titanium-dioxide films on glass, J. Mater. Res. 10 (1995) 2842–2848.
[61] S. Deng, S.W. Verbruggen, S. Lenaerts, J.A. Martens, S. Van den Berghe, K. Devloo-Casier, W. Devulder, J. Dendooven, D. Deduytsche, C. Detavernier, Controllable nitrogen doping in as deposited TiO_2 film and its effect on post deposition annealing, J. Vac. Sci. Technol. A. 32, 01A123 (2014).
[62] A. Mills, J. Hepburn, D. Hazafy, C. O'Rourke, J. Krysa, M. Baudys, M. Zlamal, H. Bartkova, C.E. Hill, K.R. Winn, M.E. Simonsen, E.G. Sogaard, S.C. Pillai, N.S. Leyland, R. Fagan, F. Neumann, C. Lampe, T. Graumann, A simple, inexpensive method for the rapid testing of the photocatalytic activity of self-cleaning surfaces, J. Photochem. Photobiol. A. 272 (2013) 18–20.
[63] M. Smits, C. Chan, T. Tytgat, B. Craeye, N. Costarramone, S. Lacombe, S. Lenaerts, Photocatalytic degradation of soot deposition: Self-cleaning effect on titanium dioxide coated cementitious materials, Chem. Eng. J. 222 (2013) 411–418.
[64] M. Smits, Y. Ling, S. Lenaerts, S. Van Doorslaer, Photocatalytic removal of soot: unravelling of the reaction mechanism by EPR and in situ FTIR spectroscopy, ChemPhysChem. 13 (2012) 4251–4257.
[65] P. Chin, G.W. Roberts, D.F. Ollis, Kinetic Modeling of photocatalyzed soot oxidation on titanium dioxide thin films, Ind. Eng. Chem. Res. 46 (2007) 7598–7604.
[66] L. Liao, S. Heylen, B. Vallaey, M. Keulemans, S. Lenaerts, M.B.J. Roeffaers, J.A. Martens, Photocatalytic carbon oxidation with nitric oxide, Appl. Catal. B. 166–167 (2015) 374–380.
[67] J. Long, S. Wang, Z. Ding, S. Wang, Y. Zhou, L. Huang, X. Wang, Amine-functionalized zirconium metal–organic framework as efficient visible-light photocatalyst for aerobic organic transformations, Chem. Commun. 48 (2012) 11656–11658.
[68] C.G. Silva, I. Luz, F.X.L.I. Xamena, A. Corma, H. Garcia, Water stable Zr-benzenedicarboxylate metal-organic frameworks as photocatalysts for hydrogen generation, Chem. Eur. J. 16 (2010) 11133–11138.
[69] R. Ameloot, M.B.J. Roeffaers, G. De Cremer, F. Vermoortele, J. Hofkens, B.F. Sels, D.E. De Vos, Metal-organic framework single crystals as photoactive matrices for the generation of metallic microstructures, Adv. Mater. 23 (2011) 1788–1791.
[70] M.D. Hernandez-Alonso, F. Fresno, S. Suarez, J.M. Coronado, Development of alternative photocatalysts to TiO_2: Challenges and opportunities, Energy Environ. Sci. 2 (2009) 1231–1257.

[71] O. Carp, C.L. Huisman, A. Reller, Photoinduced reactivity of titanium dioxide, Prog. Solid State Chem. 32 (2004) 33–177.
[72] K.W. Kolasinski, Surface Science - Foundations of Catalysis and Nanoscience, Second Edition, John Wiley & Sons Ltd, West Sussex, England, 2009.
[73] T. Van Gerven, G. Mul, J. Moulijn, A. Stankiewicz, A review of intensification of photocatalytic processes, Chem. Eng. Process. 46 (2007) 781–789.
[74] M. Pelaez, N.T. Nolan, S.C. Pillai, M.K. Seery, P. Falaras, A.G. Kontos, et al., A review on the visible light active titanium dioxide photocatalysts for environmental applications, Appl. Catal. B. 125 (2012) 331–349.
[75] A. Fujishima, T.N. Rao, D.A. Tryk, Titanium dioxide photocatalysis, J. Photochem. Photobiol. C. (2000) 1–21.
[76] H.S. Son, S.J. Lee, I.H. Cho, K.D. Zoh, Kinetics and mechanism of TNT degradation in TiO_2 photocatalysis, Chemosphere. 57 (2004) 309–317.
[77] R. Rahal, T. Pigot, D. Foix, S. Lacombe, Photocatalytic efficiency and self-cleaning properties under visible light of cotton fabrics coated with sensitized TiO_2, Appl. Catal. B. 104 (2011) 361–372.
[78] R. Rahal, M. Le Bechec, R. Guyoneaud, T. Pigot, H. Paolacci, S. Lacombe, Bactericidal activity under UV and visible light of cotton fabrics coated with anthraquinone-sensitized TiO_2, Catal. Today. 209 (2013) 134–139.
[79] C. Cantau, T. Pigot, J.C. Dupin, S. Lacombe, N-doped TiO_2 by low temperature synthesis: Stability, photo-reactivity and singlet oxygen formation in the visible range, J. Photochem. Photobiol. A. 216 (2010) 201–208.
[80] Y. Nosaka, T. Daimon, A.Y. Nosaka, Y. Murakami, Singlet oxygen formation in photocatalytic TiO_2 aqueous suspension, Phys. Chem. Chem. Phys. 6 (2004) 2917–2918.
[81] K. Ishibashi, A. Fujishima, T. Watanabe, K. Hashimoto, Quantum yields of active oxidative species formed on TiO_2 photocatalyst, J. Photochem. Photobiol. A. 134 (2000) 139–142.
[82] A. Jarandehei, M.K. Golpayegani, A. De Visscher, Kinetic modeling of photocatalytic degradation reactions: Effect of charge trapping, Appl. Catal. B. 84 (2008) 65–74.
[83] A.M. Peiro, C. Colombo, G. Doyle, J. Nelson, A. Mills, J.R. Durrant, Photochemical reduction of oxygen adsorbed to nanocrystalline TiO_2 films: A transient absorption and oxygen scavenging study of different TiO_2 preparations, J. Phys. Chem. B. 110 (2006) 23255–23263.
[84] N. Serpone, Relative photonic efficiencies and quantum yields in heterogeneous photocatalysis, J. Photochem. Photobiol. A. 104 (1997) 1–12.
[85] M.R. Hoffmann, S.T. Martin, W.Y. Choi, D.W. Bahnemann, Environmental applications of semiconductor photocatalysis, Chem. Rev. 95 (1995) 69–96.
[86] S. Brosillon, L. Lhomme, C. Vallet, A. Bouzaza, D. Wolbert, Gas phase photocatalysis and liquid phase photocatalysis: Interdependence and influence of substrate concentration and photon flow on degradation reaction kinetics, Appl. Catal. B. 78 (2008) 232–241.
[87] C. Guillard, J. Disdier, J.M. Herrmann, C. Lehaut, T. Chopin, S. Malato, J. Blanco, Comparison of various titania samples of industrial origin in the solar photocatalytic detoxification of water containing 4-chlorophenol, Catal. Today. 54 (1999) 217–228.
[88] D.E. Kritikos, N.P. Xekoukoulotakis, E. Psillakis, D. Mantzavinos, Photocatalytic degradation of reactive black 5 in aqueous solutions: Effect of operating conditions and coupling with ultrasound irradiation, Water Res. 41 (2007) 2236–2246.
[89] M. Saquib, M. Abu Tariq, M.M. Haque, M. Muneer, Photocatalytic degradation of disperse blue 1 using UV/TiO_2/H_2O_2 process, J. Environ. Manage. 88 (2008) 300–306.
[90] S.W. Verbruggen, J.J.J. Dirckx, J.A. Martens, S. Lenaerts, Surface photovoltage measurements: A quick assessment of the photocatalytic activity?, Catal. Today. 209 (2013) 215–220.
[91] K. Nakata, A. Fujishima, TiO_2 photocatalysis: Design and applications, J. Photochem. Photobiol. C. 13 (2012) 169–189.

[92] R.M. Navarro Yerga, M. Consuelo Álvarez Galván, F. del Valle, J. a. Villoria de la Mano, J.L.G. Fierro, Water splitting on semiconductor catalysts under visible light irradiation, ChemSusChem. 2 (2009) 471–485.
[93] A.J. Maira, K.L. Yeung, J. Soria, J.M. Coronado, C. Belver, C.Y. Lee, V. Augugliaro, Gas-phase photo-oxidation of toluene using nanometer-size TiO_2 catalysts, Appl. Catal. B. 29 (2001) 327–336.
[94] Y. Jiang, R. Amal, Selective synthesis of TiO_2-based nanoparticles with highly active surface sites for gas-phase photocatalytic oxidation, Appl. Catal. B. 138-139 (2013) 260–267.
[95] L. Brus, Electronic wave-functions in semiconductor clusters - experiment and theory, J. Phys. Chem. 90 (1986) 2555–2560.
[96] H. Lin, C.P. Huang, W. Li, C. Ni, S.I. Shah, Y.H. Tseng, Size dependency of nanocrystalline TiO_2 on its optical property and photocatalytic reactivity exemplified by 2-chlorophenol, Appl. Catal. B. 68 (2006) 1–11.
[97] H. Li, Z. Bian, J. Zhu, D. Zhang, G. Li, Y. Huo, H. Li, Y. Lu., Mesoporous titania spheres with tunable chamber stucture and enhanced photocatalytic activity, J. Am. Chem. Soc. 129 (2007) 8406–8407.
[98] Y. Kondo, H. Yoshikawa, K. Awaga, M. Murayama, T. Mori, K. Sunada, et al., Preparation, photocatalytic activities, and dye-sensitized solar-cell performance of submicron-scale TiO_2 hollow spheres, Langmuir. 24 (2008) 547–550.
[99] G.K. Mor, K. Shankar, M. Paulose, O.K. Varghese, C.A. Grimes, Use of highly-ordered TiO_2 nanotube arrays in dye-sensitized solar cells, Nano Lett. 6 (2006) 215–218.
[100] Y. Yuan, Y. Zhao, H. Li, Y. Li, X. Gao, C. Zheng, J. Zhang., Electrospun metal oxide-TiO_2 nanofibers for elemental mercury removal from flue gas, J. Hazard. Mater. 227-228 (2012) 427–435.
[101] Z. Wu, F. Dong, W. Zhao, H. Wang, Y. Liu, B. Guan, The fabrication and characterization of novel carbon doped TiO_2 nanotubes, nanowires and nanorods with high visible light photocatalytic activity, Nanotechnology. 20 (2009) 235701 (9p).
[102] J. Park, J. Moon, S. Lee, S.H. Kim, T. Zyung, H.Y. Chu, Structure and CO gas sensing properties of electrospun TiO_2 nanofibers, Mater. Lett. 64 (2010) 255–257.
[103] L. Francioso, A. Taurino, A. Forleo, P. Siciliano, TiO_2 nanowires array fabrication and gas sensing properties, Sensors Actuators B. 130 (2008) 70–76.
[104] T. Zhao, Z. Liu, K. Nakata, S. Nishimoto, T. Murakami, Y. Zhao, L. Jiang, A. Fujishima, Multichannel TiO_2 hollow fibers with enhanced photocatalytic activity, J. Mater. Chem. 20 (2010) 5095–5099.
[105] Z. Liu, X. Zhang, S. Nishimoto, T. Murakami, A. Fujishima, Efficient photocatalytic degradation of gaseous acetaldehyde by highly ordered TiO_2 nanotube arrays, Environ. Sci. Technol. 42 (2008) 8547–8551.
[106] T. Shibata, N. Sakai, K. Fukuda, Y. Ebina, T. Sasaki, Photocatalytic properties of titania nanostructured films fabricated from titania nanosheets, Phys. Chem. Chem. Phys. 9 (2007) 2413–2420.
[107] S. Ribbens, V. Meynen, G.V. Tendeloo, X. Ke, M. Mertens, B.U.W. Maes, P. Cool, E.F. Vansant, Development of photocatalytic efficient Ti-based nanotubes and nanoribbons by conventional and microwave assisted synthesis strategies, Microporous Mesoporous Mater. 114 (2008) 401–409.
[108] Z.Y. Yuan, J.F. Colomer, B.L. Su, Titanium oxide nanoribbons, Chem. Phys. Lett. 363 (2002) 362–366.
[109] D. Byun, Y. Jin, B. Kim, J. Kee Lee, D. Park, Photocatalytic TiO_2 deposition by chemical vapor deposition, J. Hazard. Mater. 73 (2000) 199–206.
[110] G. Li Puma, A. Bono, D. Krishnaiah, J.G. Collin, Preparation of titanium dioxide photocatalyst loaded onto activated carbon support using chemical vapor deposition: A review paper, J. Hazard. Mater. 157 (2008) 209–219.

[111] J. Sicha, J. Musil, M. Meissner, R. Cerstvy, Nanostructure of photocatalytic TiO_2 films sputtered at temperatures below 200°C, Appl. Surf. Sci. 254 (2008) 3793–3800.
[112] C. Brinker, G. Sherer, Sol-gel science: the physics and chemistry of sol-gel processing, 1990.
[113] C.J. Brinker, G.C. Frye, A.J. Hurd, C.S. Ashley, Fundamentals of sol-gel dip coating, Thin Solid Films. 201 (1991) 97–108.
[114] M. Hepel, I.D. Kumarihamy, Nanocrystalline structure and nanopore formation in modified thermal TiO_2 films, Int. J. Hydrogen Energy. 32 (2007) 2693–2702.
[115] Pilkington, Pilkington Active(TM) Product information, (2013). www.pilkington.com/activ.
[116] A. Mills, A. Lepre, N. Elliott, S. Bhopal, I.P. Parkin, S.A. O'Neill, Characterisation of the photocatalyst Pilkington Activ(TM): a reference film photocatalyst?, J. Photochem. Photobiol. A. 160 (2003) 213–224.
[117] C.Y. Wang, R. Pagel, J.K. Dohrmann, D.W. Bahnemann, Antenna mechanism and deaggregation concept: novel mechanistic principles for photocatalysis, Comptes Rendus Chim. 9 (2006) 761–773.
[118] E. Beyers, E. Biermans, S. Ribbens, K. De Witte, M. Mertens, V. Meynen, S. Bals, G. Van Tendeloo, E.F. Vansant, P.Cool, Combined TiO_2/SiO_2 mesoporous photocatalysts with location and phase controllable TiO_2 nanoparticles, Appl. Catal. B. 88 (2009) 515–524.
[119] E. Otsuka, K. Kurumada, A. Suzuki, S. Matsuzawa, K. Takeuchi, An application of transparent mesoporous bulk silica to a titanium dioxide photocatalyst with adsorption and decomposition functions, J. Sol-Gel Sci. Technol. 46 (2008) 71–78.
[120] V. Meynen, P. Cool, E.F. Vansant, Verified syntheses of mesoporous materials, Microporous Mesoporous Mater. 125 (2009) 170–223.
[121] M. Noorjahan, V.D. Kumari, M. Subrahmanyam, P. Boule, A novel and efficient photocatalyst: TiO_2-HZSM-5 combinate thin film, Appl. Catal. B. 47 (2004) 209–213.
[122] Y.M. Xu, C.H. Langford, Enhanced photoactivity of A titanium(Iv) oxide-supported on ZSM5 and zeolite-A at low-coverage, J. Phys. Chem. 99 (1995) 11501–11507.
[123] Y.M. Xu, C.H. Langford, Photoactivity of titanium dioxide supported on MCM41, zeolite X, and zeolite Y, J. Phys. Chem. B. 101 (1997) 3115–3121.
[124] X. Huang, J. Yuan, J. Shi, W. Shangguan, Ozone-assisted photocatalytic oxidation of gaseous acetaldehyde on TiO_2/H-ZSM-5 catalysts, J. Hazard. Mater. 171 (2009) 827–832.
[125] S. Sampath, H. Uchida, H. Yoneyama, Photocatalytic Degradation of Gaseous Pyridine over Zeolite-Supported Titanium Dioxide, J. Catal. 149 (1994) 189–194.
[126] N. Takeda, T. Torimoto, S. Sampath, S. Kuwabata, H. Yoneyama, Effect of inert supports for titanium-dioxide loading on enhancement of photodecomposition rate of gaseous propionaldehyde, J. Phys. Chem. 99 (1995) 9986–9991.
[127] E. Van Eynde, T. Tytgat, M. Smits, S.W. Verbruggen, B. Hauchecorne, S. Lenaerts, Biotemplated diatom silica-titania materials for air purification, Photochem. Photobiol. Sci. 12 (2012) 690–695.
[128] E. Van Eynde, B. Lenaerts, T. Tytgat, S.W. Verbruggen, B. Hauchecorne, R. Blust, et al., Effect of pretreatment and temperature on the properties of Pinnularia biosilica frustules, RSC Adv. 4 (2014) 56200–56206.
[129] A.Y. Shan, T.I.M. Ghazi, S.A. Rashid, Immobilisation of titanium dioxide onto supporting materials in heterogeneous photocatalysis: A review, Appl. Catal. A. 389 (2010) 1–8.
[130] R. Leary, A. Westwood, Carbonaceous nanomaterials for the enhancement of TiO_2 photocatalysis, Carbon 49 (2011) 741–772.
[131] C.H. Ao, S.C. Lee, Combination effect of activated carbon with TiO_2 for the photodegradation of binary pollutants at typical indoor air level, J. Photochem. Photobiol. A. 161 (2004) 131–140.
[132] C.H. Ao, S.C. Lee, Enhancement effect of TiO_2 immobilized on activated carbon filter for the photodegradation of pollutants at typical indoor air level, Appl. Catal. B. 44 (2003) 191–205.

[133] Y. Yu, J.C. Yu, J.G. Yu, Y.C. Kwok, Y.K. Che, J.C. Zhao, L. Ding, W.K. Ge, P.K. Wong, Enhancement of photocatalytic activity of mesoporous TiO_2 by using carbon nanotubes, Appl. Catal. A. 289 (2005) 186–196.
[134] N. Bouazza, M. Ouzzine, M.A. Lillo-Ródenas, D. Eder, A. Linares-Solano, TiO_2 nanotubes and CNT-TiO_2 hybrid materials for the photocatalytic oxidation of propene at low concentration, Appl. Catal. B. 92 (2009) 377–383.
[135] J. Rongé, S. Deng, S. Pulinthanathu Sree, T. Bosserez, S.W. Verbruggen, N. Kumar Singh, J. Dendooven, M.B.J. Roeffaers, F. Taulelle, M. De Volder, C. Detavernier, J.A. Martens, Air-based photoelectrochemical cell capturing water molecules from ambient air for hydrogen production, RSC Adv. 4 (2014) 29286-29290.
[136] W. Wang, P. Serp, P. Kalck, C.G. Silva, J.L. Faria, Preparation and characterization of nanostructured MWCNT-TiO_2 composite materials for photocatalytic water treatment applications, Mater. Res. Bull. 43 (2008) 958–967.
[137] Y.H. Zhang, Z.R. Tang, X.Z. Fu, Y.J. Xu, TiO_2-graphene nanocomposites for gas-phase photocatalytic degradation of volatile aromatic pollutant: Is TiO_2-graphene truly different from other TiO_2-carbon composite materials?, ACS Nano. 4 (2010) 7303–7314.
[138] T. Tytgat, Research and development of self-supporting TiO_2 foams for removal of VOCs from ambient air, PhD thesis, 2012.
[139] A.N. Kouamé, R. Masson, D. Robert, N. Keller, V. Keller, β-SiC foams as a promising structured photocatalytic support for water and air detoxification, Catal. Today. 209 (2013) 13–20.
[140] S. Hajiesmaili, S. Josset, D. Bégin, C. Pham-Huu, N. Keller, V. Keller, 3D solid carbon foam-based photocatalytic materials for vapor phase flow-through structured photoreactors, Appl. Catal. A. 382 (2010) 122–130.
[141] S. Josset, S. Hajiesmaili, D. Begin, D. Edouard, C. Pham-Huu, M. Lett, N. Keller, V. Keller, UV-A photocatalytic treatment of Legionella pneumophila bacteria contaminated airflows through three-dimensional solid foam structured photocatalytic reactors., J. Hazard. Mater. 175 (2010) 372–381.
[142] T. Tytgat, M. Smits, S. Lenaerts, S.W. Verbruggen, Immobilization of TiO_2 into self-supporting photocatalytic foam: Influence of calcination temperature, Int. J. Appl. Ceram. Technol. 11 (2014) 714-722.
[143] C. Detavernier, J. Dendooven, S. Pulinthanathu Sree, K.F. Ludwig, J.A. Martens, Tailoring nanoporous materials by atomic layer deposition, Chem. Soc. Rev. 40 (2011) 5242–5253.
[144] S. Deng, S.W. Verbruggen, Z. He, D.J. Cott, P.M. Vereecken, J.A. Martens, S. Bals, S. Lenaerts, C. Detavernier, Atomic layer deposition-based synthesis of photoactive TiO_2 nanoparticle chains by using carbon nanotubes as sacrificial templates, RSC Adv. 4 (2014) 11648-11653.
[145] S.W. Verbruggen, S. Deng, M. Kurttepeli, D.J. Cott, P.M. Vereecken, S. Bals, J.A. Martens, C. Detavernier, S. Lenaerts, Photocatalytic acetaldehyde oxidation in air using spacious TiO_2 films prepared by atomic layer deposition on supported carbonaceous sacrificial templates, Appl. Catal. B. 160-161 (2014) 204–210.
[146] M. Kurttepeli, S. Deng, S.W. Verbruggen, G. Guzzinati, D.J. Cott, S. Lenaerts, J. Verbeeck, G. Van Tendeloo, C. Detavernier, S. Bals, Synthesis and characterization of photoreactive TiO_2–carbon nanosheet composites, J. Phys. Chem. C. 118 (2014) 21031–21037.
[147] F. Sordello, C. Duca, V. Maurino, C. Minero, Photocatalytic metamaterials: TiO_2 inverse opals, Chem. Commun. 47 (2011) 6147–6149.
[148] C.L. Huisman, J. Schoonman, A. Goossens, The application of inverse titania opals in nanostructured solar cells, Sol. Energy Mater. Sol. Cells. 85 (2005) 115–124.
[149] S. Hore, P. Nitz, C. Vetter, C. Prahl, M. Niggemann, R. Kern, Scattering spherical voids in nanocrystalline TiO_2 - enhancement of efficiency in dye-sensitized solar cells, Chem. Commun. (2005) 2011–2013.
[150] C. Aprile, A. Corma, H. Garcia, Enhancement of the photocatalytic activity of TiO_2 through spatial structuring and particle size control: from subnanometric to submillimetric length scale, Phys. Chem. Chem. Phys. 10 (2008) 769–783.

[151] M. Ren, K.T. Valsaraj, Photocatalytic oxidation of gaseous 1,2-dichlorobenzene using photonic titania (inverse opal) on optical fibers in a monolith configuration, Sep. Purif. Technol. 62 (2008) 523–528.
[152] G.I.N. Waterhouse, M.R. Waterland, Opal and inverse opal photonic crystals: Fabrication and characterization, Polyhedron. 26 (2007) 356–368.
[153] E. Cho, S. Han, H.S. Ahn, K.R. Lee, S.K. Kim, C.S. Hwang, First-principles study of point defects in rutile TiO_{2-x}, Phys. Rev. B. 73 (2006) 193202 (4p.).
[154] I. Justicia, G. Garcia, L. Vázquez, J. Santiso, P. Ordejón, G. Battiston, R. Gerbasi, A. Figueras, Self-doped titanium oxide thin films for efficient visible light photocatalysis: An example: Nonylphenol photodegradation, Sensors Actuators B Chem. 109 (2005) 52–56.
[155] I. Nakamura, N. Negishi, S. Kutsuna, T. Ihara, S. Sugihara, K. Takeuchi, Role of oxygen vacancy in the plasma-treated TiO_2 photocatalyst with visible light activity for NO removal, J. Mol. Catal. A. 161 (2000) 205–212.
[156] M.S. Hamdy, R. Amrollahi, G. Mul, Surface Ti^{3+}-containing (blue) titania: A unique photocatalyst with high activity and selectivity in visible light-stimulated selective oxidation, Acs Catal. 2 (2012) 2641–2647.
[157] V. Etacheri, M.K. Seery, S.J. Hinder, S.C. Pillai, Oxygen rich titania: A dopant free, high temperature stable, and visible-light active anatase photocatalyst, Adv. Funct. Mater. 21 (2011) 3744–3752.
[158] M.I. Litter, Heterogeneous photocatalysis: Transition metal ions in photocatalytic systems, Appl. Catal. B Environ. 23 (1999) 89–114.
[159] J. Choi, H. Park, M.R. Hoffmann, Effects of single metal-ion doping on the visible-light photoreactivity of TiO_2, J. Phys. Chem. C. 114 (2010) 783–792.
[160] W.Y. Choi, A. Termin, M.R. Hoffmann, The role of metal-ion dopants in quantum-sized TiO_2 - Correlation between photoreactivity and charge-carrier recombination dynamics, J. Phys. Chem. 98 (1994) 13669–13679.
[161] B. Sun, E.P. Reddy, P.G. Smirniotis, Visible light Cr(VI) reduction and organic chemical oxidation by TiO_2 photocatalysis, Environ. Sci. Technol. 39 (2005) 6251–6259.
[162] M.S. Kang, The superhydrophilicity of Al-TiO_2 nanometer sized material synthesized using a solvothermal method, Mater. Lett. 59 (2005) 3122–3127.
[163] A.W. Xu, Y. Gao, H.Q. Liu, The preparation, characterization, and their photocatalytic activities of rare-earth-doped TiO_2 nanoparticles, J. Catal. 207 (2002) 151–157.
[164] J. Xiao, T. Peng, R. Li, Z. Peng, C. Yan, Preparation, phase transformation and photocatalytic activities of cerium-doped mesoporous titania nanoparticles, J. Solid State Chem. 179 (2006) 1161–1170.
[165] Y. Xu, H. Chen, Z. Zeng, B. Lei, Investigation on mechanism of photocatalytic activity enhancement of nanometer cerium-doped titania, Appl. Surf. Sci. 252 (2006) 8565–8570.
[166] A.M.T. Silva, C.G. Silva, G. Drazic, J.L. Faria, Ce-doped TiO_2 for photocatalytic degradation of chlorophenol, Catal. Today. 144 (2009) 13–18.
[167] Z. Liu, B. Guo, L. Hong, H. Jiang, Preparation and characterization of cerium oxide doped TiO_2 nanoparticles, J. Phys. Chem. Solids. 66 (2005) 161–167.
[168] S. Sato, Photocatalytic activity of NO_x-doped TiO_2 in the visible-light region, Chem. Phys. Lett. 123 (1986) 126–128.
[169] S. Sato, R. Nakamura, S. Abe, Visible-light sensitization of TiO_2 photocatalysts by wet-method N doping, Appl. Catal. A. 284 (2005) 131–137.
[170] A. V. Emeline, V.N. Kuznetsov, V.K. Rybchuk, N. Serpone, Visible-light-active titania photocatalysts: The case of N-doped TiO_2s—Properties and some fundamental issues, Int. J. Photoenergy. 2008 (2008) 1–19.
[171] D. Li, H. Haneda, S. Hishita, N. Ohashi, Visible-light-driven N-F-codoped TiO_2 photocatalysts. 2. Optical characterization, photocatalysis, and potential application to air purification, Chem. Mater. 17 (2005) 2596–2602.

[172] J. Shang, W.Q. Yao, Y.F. Zhu, N.Z. Wu, Structure and photocatalytic performances of glass/SnO_2/TiO_2 interface composite film, Appl. Catal. A. 257 (2004) 25–32.
[173] A. Hattori, Y. Tokihisa, H. Tada, S. Ito, Acceleration of oxidations and retardation of reductions in photocatalysis of a TiO_2/SnO_2 bilayer-type catalyst, J. Electrochem. Soc. 147 (2000) 2279–2283.
[174] M. Miyauchi, A.K. Nakajima, T. Watanabe, K. Hashimoto, Photoinduced hydrophilic conversion of TiO_2/WO_3 layered thin films, Chem. Mater. 14 (2002) 4714–4720.
[175] A. Fuerte, M.D. Hernandez-Alonso, A.J. Maira, A. Martinez-Arias, M. Fernandez-Garcia, J.C. Conesa, J. Soria, G. Munuera, Nanosize Ti-W mixed oxides: Effect of doping level in the photocatalytic degradation of toluene using sunlight-type excitation, J. Catal. 212 (2002) 1–9.
[176] R. Su, R. Bechstein, L. So, R.T. Vang, M. Sillassen, B. Esbjornsson, A. Palmqvist, F. Besenbacher, How the anatase-to-rutile ratio influences the photoreactivity of TiO_2, J. Phys. Chem. C. 115 (2011) 24287–24292.
[177] R.I. Bickley, T. Gonzalezcarreno, J.S. Lees, L. Palmisano, R.J.D. Tilley, A structural investigation of titanium-dioxide photocatalysts, J. Solid State Chem. 92 (1991) 178–190.
[178] G.H. Li, C.P. Richter, R.L. Milot, L. Cai, C.A. Schmuttenmaer, R.H. Crabtree, G.W. Brudvig, V.S. Batista, Synergistic effect between anatase and rutile TiO_2 nanoparticles in dye-sensitized solar cells, Dalt. Trans. (2009) 10078–10085.
[179] Y.K. Kho, A. Iwase, W.Y. Teoh, L. Madler, A. Kudo, R. Amal, Photocatalytic H_2 evolution over TiO_2 nanoparticles. The synergistic effect of anatase and rutile, J. Phys. Chem. C. 114 (2010) 2821–2829.
[180] D.C. Hurum, A.G. Agrios, K.A. Gray, T. Rajh, M.C. Thurnauer, Explaining the enhanced photocatalytic activity of Degussa P25 mixed-phase TiO_2 using EPR, J. Phys. Chem. B. 107 (2003) 4545–4549.
[181] T. Ohno, K. Sarukawa, K. Tokieda, M. Matsumura, Morphology of a TiO_2 photocatalyst (Degussa, P-25) consisting of anatase and rutile crystalline phases, J. Catal. 203 (2001) 82–86.
[182] B. Ohtani, O.O. Prieto-Mahaney, D. Li, R. Abe, What is Degussa (Evonik) P25? Crystalline composition analysis, reconstruction from isolated pure particles and photocatalytic activity test, J. Photochem. Photobiol. A Chem. 216 (2010) 179–182.
[183] R.A. Larson, P.L. Stackhouse, T.O. Crowley, Riboflavin tetraacetate - A potentially useful photosensitizing agent for the treatment of contaminated waters, Environ. Sci. Technol. 26 (1992) 1792–1798.
[184] B. O'Regan, M. Grätzel, A low-cost, high-efficiency solar-cell based on dye-sensitized colloidal TiO_2 films, Nature. 353 (1991) 737–740.
[185] H.N. Chen, W.P. Li, H.C. Liu, L.Q. Zhu, Performance enhancement of CdS-sensitized TiO_2 mesoporous electrode with two different sizes of CdS nanoparticles, Microporous Mesoporous Mater. 138 (2011) 235–238.
[186] R. Abe, K. Hara, K. Sayama, K. Domen, H. Arakawa, Steady hydrogen evolution from water on Eosin Y-fixed TiO_2 photocatalyst using a silane-coupling reagent under visible light irradiation, J. Photochem. Photobiol. A. 137 (2000) 63–69.
[187] T. Puangpetch, P. Sommakettarin, S. Chavadej, T. Sreethawong, Hydrogen production from water splitting over Eosin Y-sensitized mesoporous-assembled perovskite titanate nanocrystal photocatalysts under visible light irradiation, Int. J. Hydrogen Energy. 35 (2010) 12428–12442.
[188] K. Whitehead, J.I. Hedges, Photodegradation and photo sensitization of mycosporine-like amino acids, J. Photochem. Photobiol. B-Biology. 80 (2005) 115–121.
[189] J.P. Escalada, A. Pajares, J. Gianotti, W.A. Massad, S. Bertolotti, F. Amat-Guerri, N.A. Garcia, Dye-sensitized photodegradation of the fungicide carbendazim and related benzimidazoles, Chemosphere. 65 (2006) 237–244.
[190] R. Abe, K. Sayama, H. Arakawa, Dye-sensitized photocatalysts for efficient hydrogen production from aqueous I- solution under visible light irradiation, J. Photochem. Photobiol. A. 166 (2004) 115–122.

[191] K. Demeestere, J. Dewulf, T. Ohno, P.H. Salgado, H. Van Langenhove, Visible light mediated photocatalytic degradation of gaseous trichloroethylene and dimethyl sulfide on modified titanium dioxide, Appl. Catal. B Environ. 61 (2005) 140–149.
[192] H. Wang, Y. Bai, H. Zhang, Z. Zhang, J. Li, L. Guo, CdS quantum dots-sensitized TiO_2 nanorod array on transparent conductive glass photoelectrodes, J. Phys. Chem. C. 114 (2010) 16451–16455.
[193] Y.L. Lee, C.F. Chi, S.Y. Liau, CdS/CdSe co-sensitized TiO_2 photoelectrode for efficient hydrogen generation in a photoelectrochemical Cell, Chem. Mater. 22 (2010) 922–927.
[194] D.R. Baker, P. V Kamat, Photosensitization of TiO_2 nanostructures with CdS quantum dots: Particulate versus tubular support architectures, Adv. Funct. Mater. 19 (2009) 805–811.
[195] H. Lee, H.C. Leventis, S.J. Moon, P. Chen, S. Ito, S.A. Haque, et al., PbS and US quantum dot-sensitized solid-state solar cells: "Old concepts, new results," Adv. Funct. Mater. 19 (2009) 2735–2742.
[196] N. Balis, V. Dracopoulos, K. Bourikas, P. Lianos, Quantum dot sensitized solar cells based on an optimized combination of ZnS, CdS and CdSe with CoS and CuS counter electrodes, Electrochim. Acta. 91 (2013) 246–252.
[197] D. Liu, R.W. Fessenden, G.L. Hug, P. V Kamat, Dye capped semiconductor nanoclusters. Role of back electron transfer in the photosensitization of SnO_2 nanocrystallites with cresyl violet aggregates, J. Phys. Chem. B. 101 (1997) 2583–2590.
[198] F. Liu, G.J. Meyer, Remote and adjacent excited-state electron transfer at TiO_2 interfaces sensitized to visible light with Ru(II) compounds, Inorg. Chem. 44 (2005) 9305–9313.
[199] G. Sauve, M.E. Cass, G. Coia, S.J. Doig, I. Lauermann, K.E. Pomykal, N.S. Lewis, Dye sensitization of nanocrystalline titanium dioxide with osmium and ruthenium polypyridyl complexes, J. Phys. Chem. B. 104 (2000) 6821–6836.
[200] P. Jarosz, P.W. Du, J. Schneider, S.H. Lee, D. McCamant, R. Eisenberg, Platinum(II) terpyridyl acetylide complexes on platinized TiO_2: Toward the photogeneration of H_2 in aqueous media, Inorg. Chem. 48 (2009) 9653–9663.
[201] S. Link, M.A. El-Sayed, Size and temperature dependence of the plasmon absorption of colloidal gold nanoparticles, J. Phys. Chem. B. 103 (1999) 4212–4217.
[202] J. Homola, S.S. Yee, G. Gauglitz, Surface plasmon resonance sensors: review, Sensors Actuators B Chem. 54 (1999) 3–15.
[203] H.A. Atwater, A. Polman, Plasmonics for improved photovoltaic devices, Nat. Mater. 9 (2010) 205–213.
[204] M. Eghtedari, A. Oraevsky, J.A. Copland, N.A. Kotov, A. Conjusteau, M. Motamedi, High sensitivity of in vivo detection of gold nanorods using a laser optoacoustic imaging system, Nano Lett. 7 (2007) 1914–1918.
[205] I.H. El-Sayed, X.H. Huang, M.A. El-Sayed, Surface plasmon resonance scattering and absorption of anti-EGFR antibody conjugated gold nanoparticles in cancer diagnostics: Applications in oral cancer, Nano Lett. 5 (2005) 829–834.
[206] S. Habuchi, M. Cotlet, R. Gronheid, G. Dirix, J. Michiels, J. Vanderleyden, F.C. De Schryver, J. Hofkens, Single-molecule surface enhanced resonance Raman spectroscopy of the enhanced green fluorescent protein, J. Am. Chem. Soc. 125 (2003) 8446–8447.
[207] K.G.M. Laurier, M. Poets, F. Vermoortele, G. De Cremer, J.A. Martens, H. Uji-i, D.E. De Vos, J. Hofkens, M.B.J. Roeffaers, Photocatalytic growth of dendritic silver nanostructures as SERS substrates, Chem. Commun. 48 (2012) 1559–1561.
[208] E. Kowalska, O.O.P. Mahaney, R. Abe, B. Ohtani, Visible-light-induced photocatalysis through surface plasmon excitation of gold on titania surfaces, Phys. Chem. Chem. Phys. 12 (2010) 2344–2355.
[209] X.M. Zhou, G. Liu, J.G. Yu, W.H. Fan, Surface plasmon resonance-mediated photocatalysis by noble metal-based composites under visible light, J. Mater. Chem. 22 (2012) 21337–21354.
[210] X. Zhang, Y.L. Chen, R. Liu, D.P. Tsai, Plasmonic photocatalysis, Reports Prog. Phys. 76 (2013) 046401 (41p.).

[211] G. Artioli, I. Angelini, A. Polla, Crystals and phase transitions in protohistoric glass materials, Phase Transitions. 81 (2008) 233–252.
[212] O. Bobin, M. Schvoerer, C. Ney, M. Rammah, B. Pannequin, E.C. Platamone, A. Daoulatli, R.P. Gayraud, The role of copper and silver in the colouration of metallic luster decorations (Tunisia, 9th Century; Mesopotamia, 10th Century; Sicily, 16th Century): A first approach, Color Res. Appl. 28 (2003) 352–359.
[213] G. Mie, Beiträge zur Optik trüber Medien, speziell kolloidaler Metallösungen, Ann. Phys. 330 (1908) 377–445.
[214] D.D. Evanoff, G. Chumanov, Size-controlled synthesis of nanoparticles. 2. Measurement of extinction, scattering, and absorption cross sections, J. Phys. Chem. B. 108 (2004) 13957–13962.
[215] C.A. Leatherdale, W.K. Woo, F. V Mikulec, M.G. Bawendi, On the absorption cross section of CdSe nanocrystal quantum dots, J. Phys. Chem. B. 106 (2002) 7619–7622.
[216] M.A. Garcia, Surface plasmons in metallic nanoparticles: fundamentals and applications, J. Phys. D. Appl. Phys. 44 (2011) 283001 (20p.).
[217] L.M. Liz-Marzan, Tailoring surface plasmons through the morphology and assembly of metal nanoparticles, Langmuir. 22 (2006) 32–41.
[218] S.W. Verbruggen, M. Keulemans, J.A. Martens, S. Lenaerts, Predicting the surface plasmon resonance wavelength of gold-silver alloy nanoparticles, J. Phys. Chem. C. 117 (2013) 19142–19145.
[219] S. Eustis, M.A. El-Sayed, Why gold nanoparticles are more precious than pretty gold: Noble metal surface plasmon resonance and its enhancement of the radiative and nonradiative properties of nanocrystals of different shapes, Chem. Soc. Rev. 35 (2006) 209–217.
[220] M. Hu, J.Y. Chen, Z.Y. Li, L. Au, G. V Hartland, X.D. Li, et al., Gold nanostructures: engineering their plasmonic properties for biomedical applications, Chem. Soc. Rev. 35 (2006) 1084–1094.
[221] L.J. Sherry, S.H. Chang, G.C. Schatz, R.P. Van Duyne, B.J. Wiley, Y. Xia, Localized surface plasmon resonance spectroscopy of single silver nanocubes, Nano Lett. 5 (2005) 2034–2038.
[222] H. Ditlbacher, A. Hohenau, D. Wagner, U. Kreibig, M. Rogers, F. Hofer, F.R. Aussenegg, J.R. Krenn, Silver nanowires as surface plasmon resonators, Phys. Rev. Lett. 95 (2005) 257403.
[223] S.W. Verbruggen, M. Keulemans, M. Filippousi, D. Flahaut, G. Van Tendeloo, S. Lacombe, J.A. Martens, S. Lenaerts, Plasmonic gold–silver alloy on TiO_2 photocatalysts with tunable visible light activity, Appl. Catal. B Environ. 156–157 (2014) 116–121.
[224] Z.W. Liu, W.B. Hou, P. Pavaskar, M. Aykol, S.B. Cronin, Plasmon resonant enhancement of photocatalytic water splitting under visible illumination, Nano Lett. 11 (2011) 1111–1116.
[225] C.G. Silva, R. Juárez, T. Marino, R. Molinari, H. García, Influence of excitation wavelength (UV or visible light) on the photocatalytic activity of titania containing gold nanoparticles for the generation of hydrogen or oxygen from water., J. Am. Chem. Soc. 133 (2011) 595–602.
[226] S. Linic, P. Christopher, D.B. Ingram, Plasmonic-metal nanostructures for efficient conversion of solar to chemical energy, Nat. Mater. 10 (2011) 911–921.
[227] D. Tsukamoto, A. Shiro, Y. Shiraishi, Y. Sugano, S. Ichikawa, S. Tanaka, T. Hirai, Photocatalytic H_2O_2 production from ethanol/O_2 system using TiO_2 loaded with Au-Ag bimetallic alloy nanoparticles, Acs Catal. 2 (2012) 599–603.
[228] Y. Tian, T. Tatsuma, Plasmon-induced photoelectrochemistry at metal nanoparticles supported on nanoporous TiO_2, Chem. Commun. (2004) 1810–1811.
[229] Y. Tian, T. Tatsuma, Mechanisms and applications of plasmon-induced charge separation at TiO_2 films loaded with gold nanoparticles, J. Am. Chem. Soc. 127 (2005) 7632–7637.
[230] K. Awazu, M. Fujimaki, C. Rockstuhl, J. Tominaga, H. Murakami, Y. Ohki, N. Yoshida, T. Watanabe, A plasmonic photocatalyst consisting of sliver nanoparticles embedded in titanium dioxide, J. Am. Chem. Soc. 130 (2008) 1676–1680.
[231] M.K. Kumar, S. Krishnamoorthy, L.K. Tan, S.Y. Chiam, S. Tripathy, H. Gao, Field effects in plasmonic photocatalyst by precise SiO_2 thickness control using atomic layer deposition, Acs Catal. 1 (2011) 300–308.

[232] R. Amrollahi, M.S. Hamdy, G. Mul, Understanding promotion of photocatalytic activity of TiO_2 by Au nanoparticles, J. Catal. 319 (2014) 194–199.
[233] P. Christopher, H.L. Xin, S. Linic, Visible-light-enhanced catalytic oxidation reactions on plasmonic silver nanostructures, Nat. Chem. 3 (2011) 467–472.
[234] D.D. Evanoff, G. Chumanov, Synthesis and optical properties of silver nanoparticles and arrays, ChemPhysChem. 6 (2005) 1221–1231.
[235] J.R. Adleman, D.A. Boyd, D.G. Goodwin, D. Psaltis, Heterogenous catalysis mediated by plasmon heating., Nano Lett. 9 (2009) 4417–23.
[236] M.J. Kale, T. Avanesian, P. Christopher, Direct photocatalysis by plasmonic nanostructures, ACS Catal. 4 (2014) 116–128.
[237] H. Nishi, T. Torimoto, T. Tatsuma, Wavelength- and efficiency-tunable plasmon-induced charge separation by the use of Au–Ag alloy nanoparticles, Phys. Chem. Chem. Phys. 17 (2015) 4042–4046.
[238] V. Subramanian, E.E. Wolf, P. V Kamat, Catalysis with TiO_2/gold nanocomposites. Effect of metal particle size on the Fermi level equilibration, J. Am. Chem. Soc. 126 (2004) 4943–4950.
[239] A. Takai, P. V. Kamat, Capture, store, and discharge. Shuttling photogenerated electrons across TiO_2-silver interface, ACS Nano. 5 (2011) 7369–7376.
[240] P. V Kamat, Manipulation of charge transfer across semiconductor interface. A criterion that cannot be ignored in photocatalyst design, J. Phys. Chem. Lett. 3 (2012) 663–672.
[241] J. Mo, Y. Zhang, Q. Xu, J.J. Lamson, R. Zhao, Photocatalytic purification of volatile organic compounds in indoor air: A literature review, Atmos. Environ. 43 (2009) 2229–2246.
[242] J. Zhao, X. Yang, Photocatalytic oxidation for indoor air purification: a literature review, Build. Environ. 38 (2003) 645–654.
[243] Y. Luo, D.F. Ollis, Heterogeneous photocatalytic oxidation of trichloroethylene and toluene mixtures in air: Kinetic promotion and inhibition, time-dependent catalyst activity, J. Catal. 163 (1996) 1–11.
[244] T.N. Obee, S.O. Hay, Effects of moisture and temperature on the photooxidation of ethylene on Titania, Environ. Sci. Technol. 31 (1997) 2034–2038.
[245] W.H. Chen, J.S. Zhang, Photocatalytic oxidation of multi-component systems - An investigation using toluene/ethylbenzene, octane/decane/dodecane and formaldehyde/acetaldehyde, J. Adv. Oxid. Technol. 11 (2008) 163–173.
[246] S. Yamazaki-Nishida, X. Fu, M.A. Anderson, K. Hori, Chlorinated byproducts from the photoassisted catalytic oxidation of trichloroethylene and tetrachloroethylene in the gas phase using porous TiO_2 pellets, J. Photochem. Photobiol. A Chem. 97 (1996) 175–179.
[247] W.J. Fisk, Health and productivity gains from better indoor environments and their relationship with building energy efficiency, Annu. Rev. Energy Environ. 25 (2000) 537–566.
[248] BCC Research, Photocatalysts: technologies and global markets, Rep. Code AVM069A. (2010).
[249] S. Verbruggen, T. Tytgat, S. Van Passel, J. Martens, S. Lenaerts, Cost-effectiveness analysis to assess commercial TiO_2 photocatalysts for acetaldehyde degradation in air, Chem. Pap. 68 (2014) 1273–1278.
[250] S.W. Verbruggen, S. Lenaerts, S. Denys, Analytic versus CFD approach for kinetic modeling of gas phase photocatalysis, Chem. Eng. J. 262 (2015) 1–8.

Figure Captions

Figure 1. ***Deaths (per 100,000) attributable to outdoor air pollution (2008).*** **©World Health Organization ref.** [1]

Figure 2. ***Number of publications on gas phase photocatalysis as a function of the year of publication according to an ISI Web of Knowledge search with the keyword combinations*** **photocat*** ***AND*** **air** ***(black bars), and*** **photocat*** ***AND*** **gas*** ***(grey bars).***

Figure 3. ***Crystal structure of a) TiO_2 anatase and b) TiO_2 rutile.*** **(color version online)**

Figure 4. ***Schematic representation of the TiO_2 band structure with indication of the redox potentials of photogenerated holes and electrons (vs. SHE) at neutral pH. As an example, the required redox potentials are indicated for the water splitting reaction (grey) or the formation of reactive oxygen radicals for photocatalytic degradation reactions (dark orange).*** **Based on the values reported in ref.**[75]**. (color version online)**

Figure 5. ***Morphological classification of photocatalyst materials based on their dimensionality. A*****dapted from ref.**[91] **©2012 with permission from Elsevier. (color version online)**

Figure 6. ***Electron microscopy pictures of a) aligned TiO_2 nanotube arrays, b) TiO_2 nanofibers and c) hollow TiO_2 nanofibers with no, one, two and three channels.***
a) reprinted with permission from ref.[99] **©2006 American Chemical Society, b) reprinted with permission from ref.**[100] **©2012 Elsevier and c) reprinted with permission from ref.** [104]**©2010 The Royal Society of Chemistry.**

Figure 7. ***a) SiO_2 diatom frustule support and b) macroscopic self-supporting TiO_2 foams.*** **a) reproduced from ref.**[127] **©2012 with permission of The Royal Society of Chemistry. b) reproduced from ref.**[138] **with permission from the author. (color version online)**

Figure 8. ***Picture of 10 µm CNT template with increasing number of TiO_2 deposition cycles by ALD after annealing (a) and increasing number of TiO_2 deposition cycles by ALD on CNS template after annealing (b), cross section SEM image of TiO_2 PC500 reference film (Crystal Global) (c), SEM image of 200 TiO_2 ALD cycles on CNS template as deposited (d), after calcination (e) and TEM details of the latter (f). Cross section SEM image of 100 TiO_2 ALD cycles on CNT template as deposited (g), after calcination (h) and TEM details of the latter (i).*** **Reprinted with permission from ref.**[145] **©2014 Elsevier. (color version online)**

Figure 9. ***SEM image of an ordered TiO_2 inverse opal film with a schematic illustration of the increase in effective light path length in the photonic structure.*** **Adapted with permission from ref.**[152] **©2007 Elsevier. (color version online)**

Figure 10. ***Schematic illustration of the effect of doping with cations (dopant energy level arbitrarily chosen) and anions on the band gap.*** **(color version online)**

Figure 11. ***Schematic representation of the vectorial charge transfer in a TiO_2/SnO_2 composite semiconductor***

Figure 12. D
emonstration of the synergetic effect of co-presence of anatase and rutile. **Adapted with permission from ref.**[176] **©2011 American Chemical Society. (color version online)**

Figure 13. ***a) Schematic representation of electron flow and mechanism of photosensitization. b) TiO_2 nanorod decorated with CdS quantum dots.*** **Panel b reprinted with permission from ref.**[192] **©2010 American Chemical Society. (color version online)**

Figure 14. **Lycurgus** ***Cup dating from the 4th century (AD) as it is (left) and under illumination (right).*** **Picture: British Museum Images. (color version online)**

Figure 15. ***Simulated extinction spectra of a) 10 nm silver and gold nanoparticles in air, b) silver nanoparticles in air of different sizes, and c) 10 nm Ag nanoparticles in air and water.*** **simulated using MiePlot v4300. (color version online)**

Figure 16. ***Photographs of $Au_xAg_{(1-x)}$ with x from left to right 0.2, 0.4, 0.6, 0.8 and 1.0 of a) colloidal alloy nanoparticle solutions and b) plasmonic photocatalyst powders obtained after photodeposition of the colloidal nanoparticles on TiO_2. Corresponding UV-VIS absorption spectra of c) colloidal $Au_xAg_{(1-x)}$ nanoparticle solutions and d) plasmonic $Au_xAg_{(1-x)}$-TiO_2 photocatalysts (the gray curve corresponds to crude TiO_2). STEM-EDX maps of e) 100% gold nanoparticles on TiO_2 (Au: red, Ti: green) and f) and $Au_{0.6}Ag_{0.4}$ alloy nanoparticle on TiO_2.*** **Reprinted with permission from ref.** [223] **©2014 Elsevier. (color version online)**

Figure 17. ***Potential mechanisms of plasmon-mediated photocatalysis. a) Direct charge injection of an electron from a plasmon excited state on the metal into the semiconductor's conduction band. b) Near-field enhancement close to the***

plasmonic metal surface. c) Extension of the effective optical path length by means of multiple scattering. **Panel b reprinted with permission from ref.**[224] **©2011 American Chemical Society. (color version online)**

Figure 1 (double column)

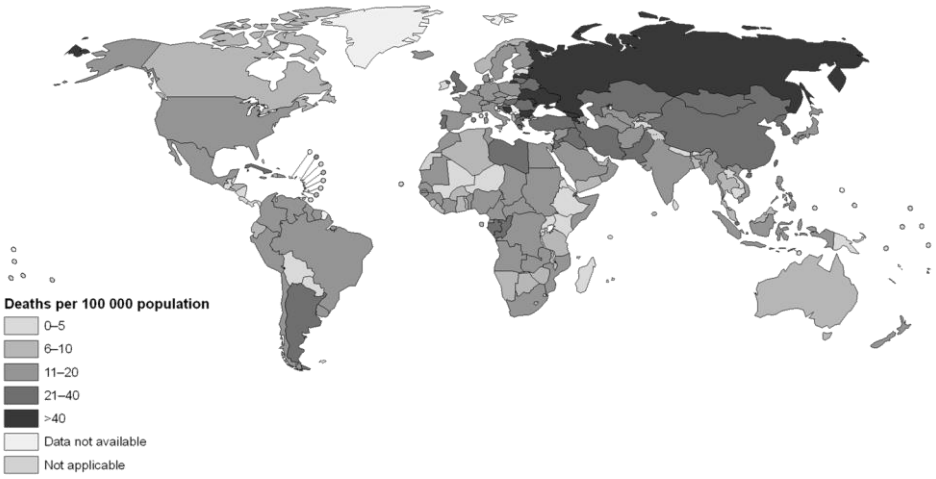

Figure 2 (single column)

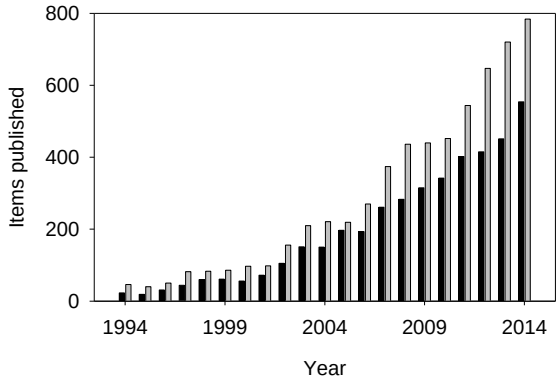

Figure 3 (single column, color online)

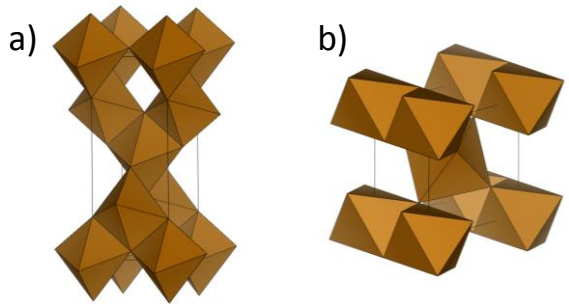

Figure 4 (single column, color online)

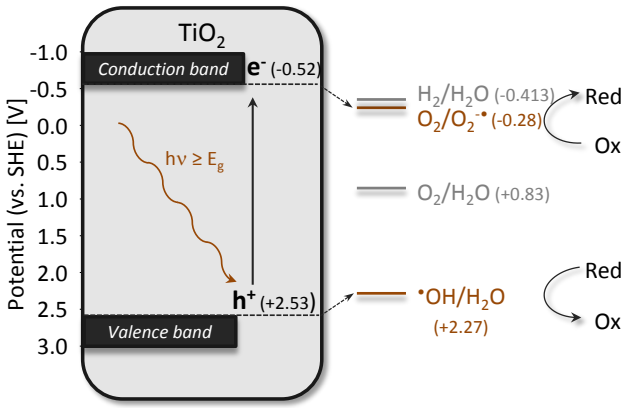

Figure 5 (single column, color online)

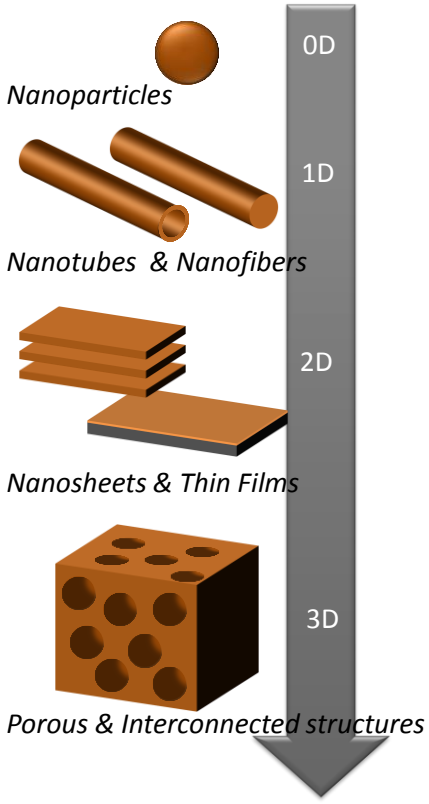

Figure 6 (single column)

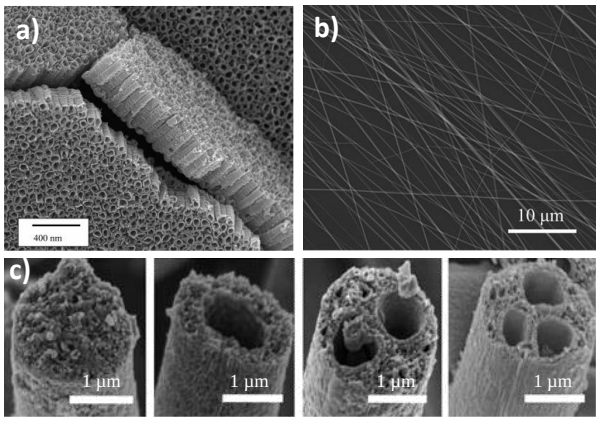

Figure 7 (single column, color online)

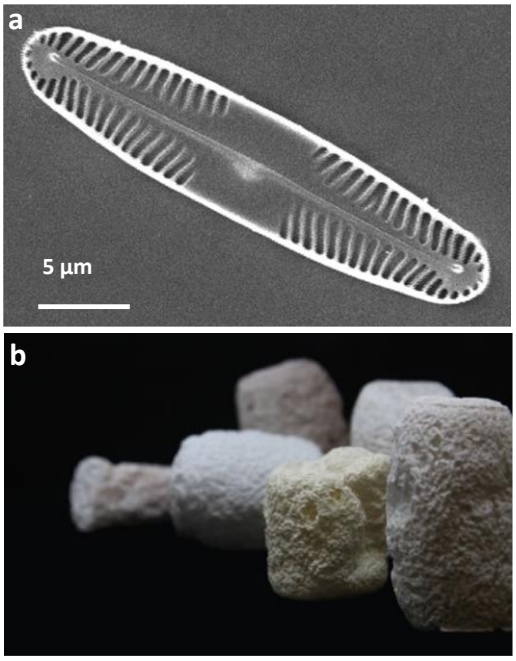

Figure 8 (double column, color online)

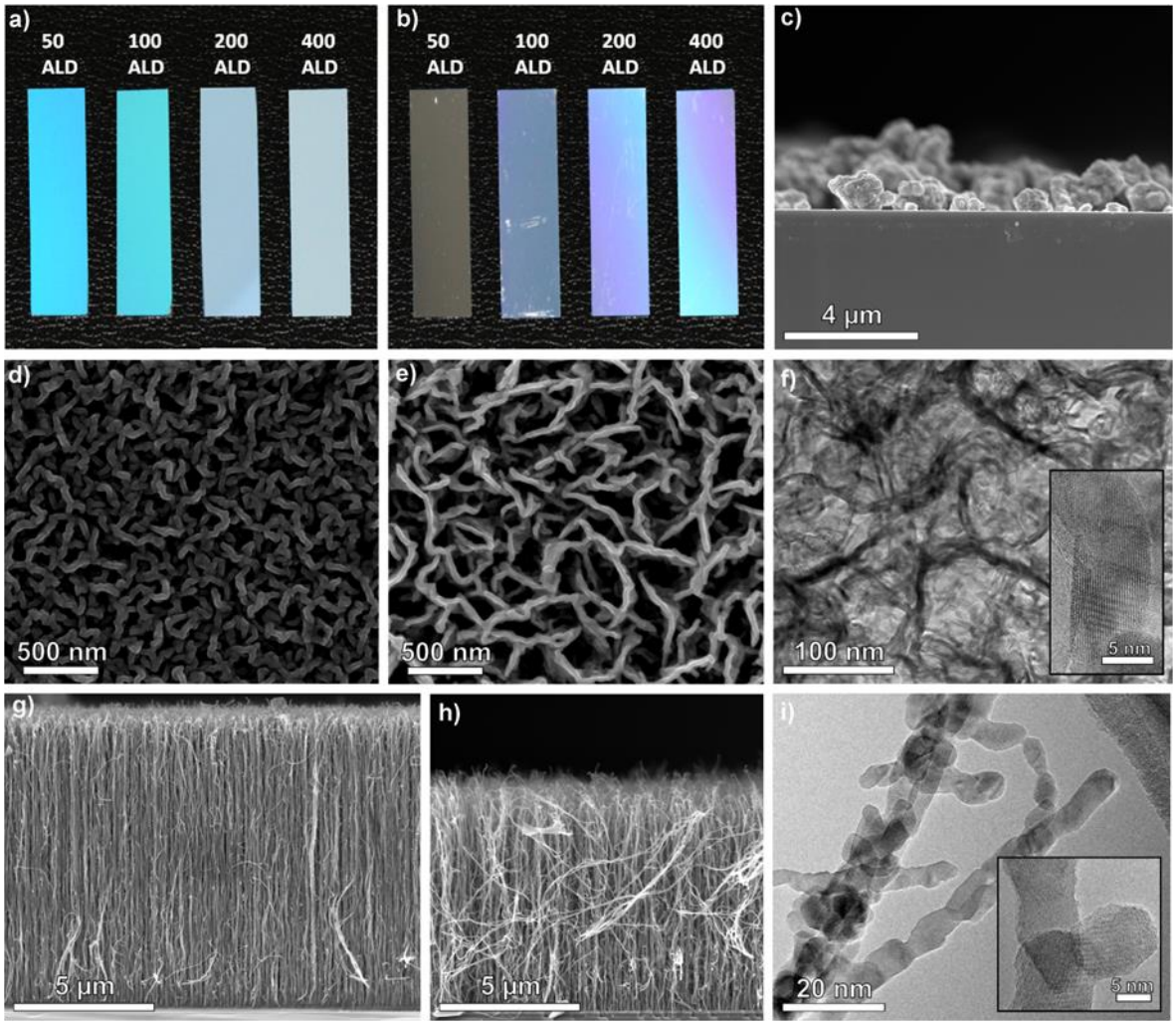

Figure 9 (single column, color online)

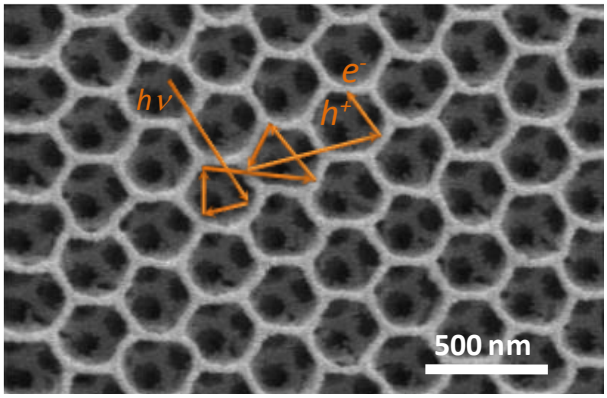

Figure 10 (double column, color online)

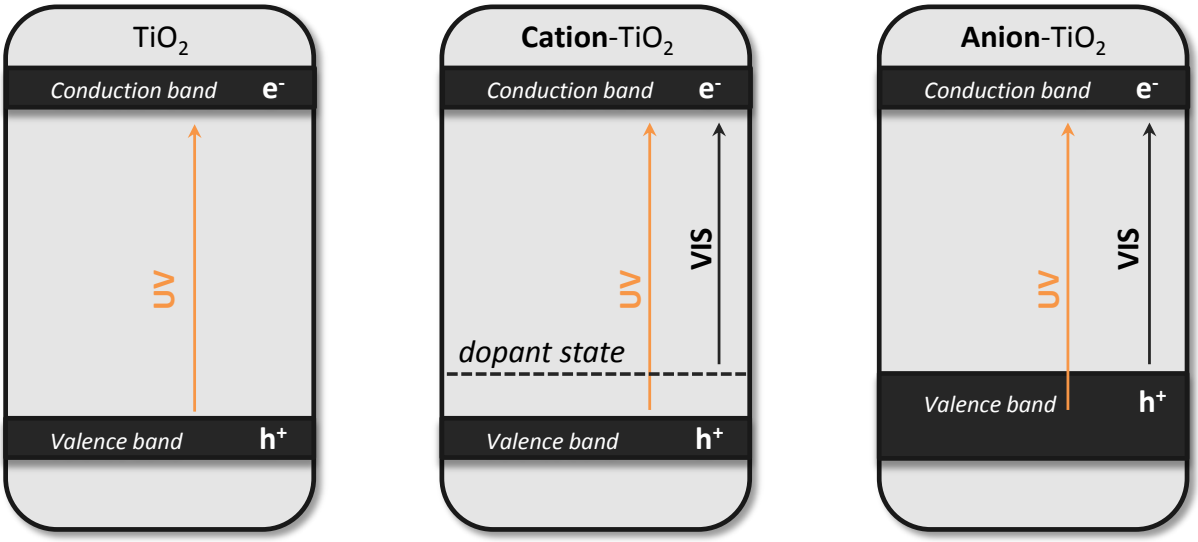

Figure 11 (single column, color online)

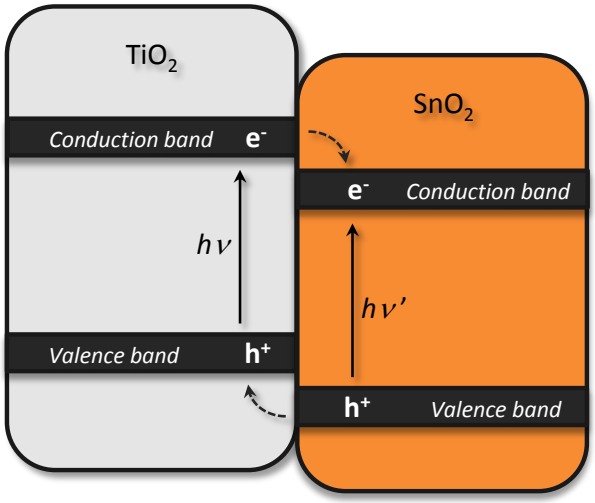

Figure 12 (single column, color online)

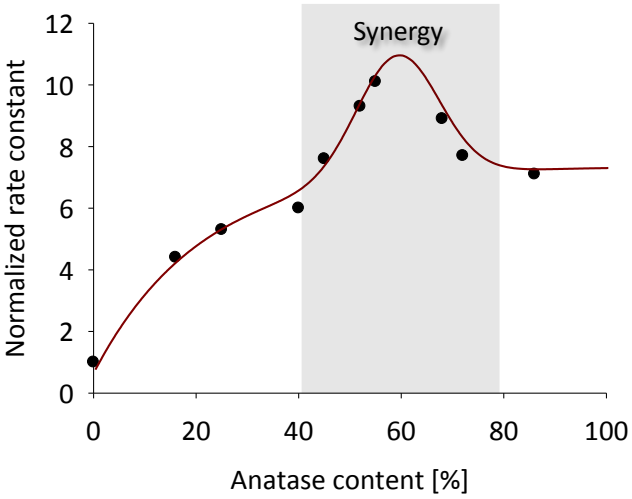

Figure 13 (single column, color online)

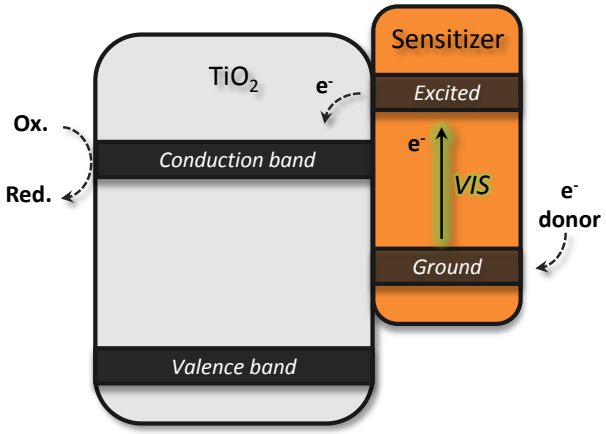

b)

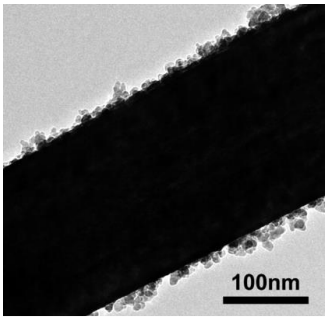

Figure 14 (single column, color online)

Figure 15 (double column, color online)

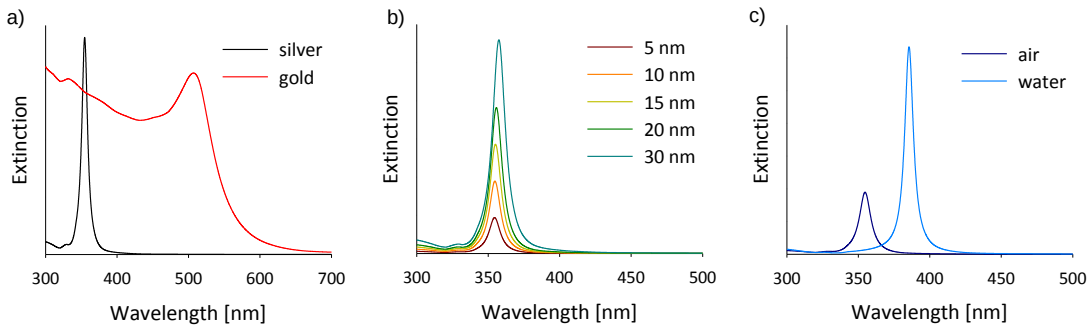

Figure 16 (single column, color online)

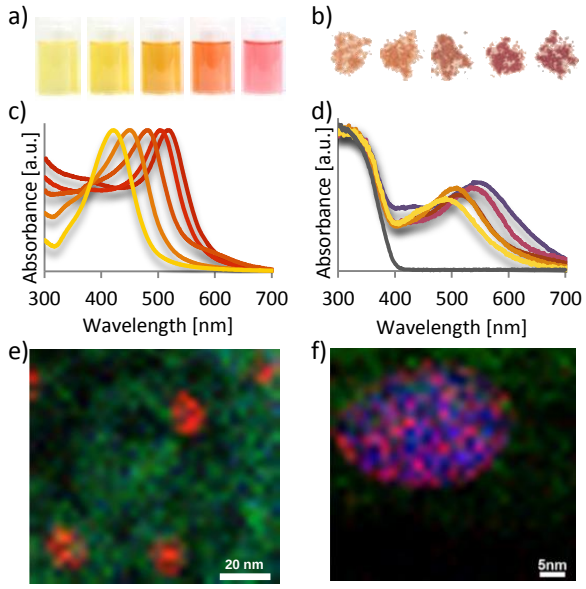

Figure 17 (single column, color online)

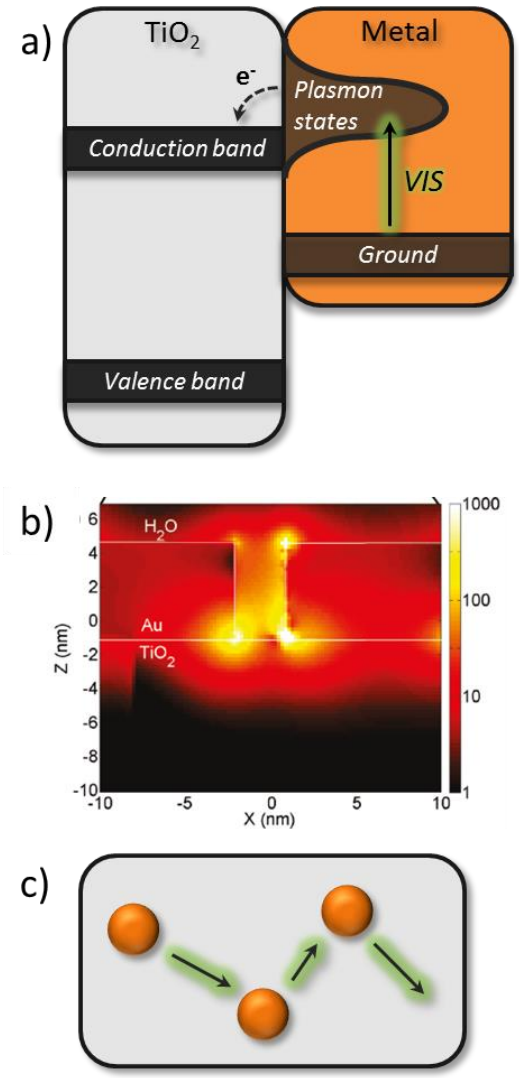

Table 1. ***Selected examples of pollutants degraded by PCO on TiO_2-based photocatalysts in gaseous environment***

Pollutant class	Compound	Catalyst [a]	Concentration [b]	Absolute intensity [b]	(Best) achievement [c]	Reference
NO_x	NO	P25	5 ppm	0.2 - 0.8 mW/cm²	70% conversion	Devahasdin [22]
		TiO_2-NH_3	200 ppb	750 µW/cm²	76.6% conversion	Li [23]
		Aerolyst 7710	5000 ppm	*not specified*	Mechanistic elucidation	Hauchecorne [24]
	NO/NO_2	*TiO_2, not specified*	10-100 ppm	*not specified*	Surface reaction by XPS	Dalton [25]
		23% TiO_2/Al_2O_3	48 ppm	Only distribution given	320 µmol/g catalyst	Shelimov [26]
SO_x	SO_2	TiO_2 on asphalt	175 ppb	2 mW/cm²	23% conversion	Hassan [27]
		Synthesized TiO_2	2529 mg/m³	*not specified*	98% conversion	Zhao [28]
VOCs						
Alkanes	Isooctane	P25	400 ppmv	7.56 x 10^{-9} E/cm²/s	98.9% conversion	Alberici [29]
	Cyclohexane	P25	250 ppm	*not specified*	66% → 57% conversion	Einaga [30]
Halo-alkanes	Dichloromethane	0.005 mol% Fe-TiO_2	96 ppm	0.83 mW/cm²	87% conversion	Hung [31]
	Chloroform	Synthesized TiO_2	162.6 ppmv	1.7 x 10^{-7} E/s	90%, fast deactivation	Yamazaki [32]
Alkenes	Ethylene	Aerolyst 7710	100 ppmv	640 µW/cm² @ 254 nm	100% conversion	Tytgat [33]
		Aerolyst on beads	75 ppmv	1.3 mW/cm² @ 254 nm	97% conversion	Verbruggen [34]
	Propene	P25	100 ppmv	*not specified*	100% conversion	Bouazza [35]
	1-butene	Synthesized TiO_2	2.75 ppm	0.70 mW/cm²	0.4 µmol/cm²/h	Cao [36]
	1,3-butadiene	P25	~ 40 ppmv	0.009 W/cm²	0.65 µmol/cm²/h	Obee [37]
Halo-alkenes	1,2-cis-dichloroethylene	TiO_2 fiberglass cloth	1000 ppmv	1 mW/cm²	96% conversion to CO_2	Ozaki [38]
	Trichloroethylene	Synthesized TiO_2	240 ppm	*not specified*	1.7 µmol/s/g	Maira [39]
	Tetrachloroethylene	*TiO_2, not specified*	16.5 g/m³	32.6 mW/cm²	56.7% conversion	Hager [40]
Aldehydes	Formaldehyde	P25	~ 45 ppmv	0.0093 W/cm²	10 µmol/cm²/h	Obee [37]
	Acetaldehyde	PC500	170 ppmv	205 µW/cm² @ 365 nm	99% conversion	Verbruggen [41]
	Butyraldehyde	P25	118 mg/m³	5 x 10^{-7} E/cm²/min	1.5 µg/cm²	Peral [42]
Alcohols	Methanol	Synthesized TiO_2	300 ppm	2.095 mW/cm²	~1.7 x 10^3 mol/m³/min	Kim [43]

	Ethanol	Synthesized TiO_2	*Not specified, spike vapors*	0.12 mW/cm²	Mechanistic elucidation	Coronado [44]
	2-propanol	PC500	400 ppbv	3.2 mW/cm²	96% mineralization	Vildozo [45]
	1-butanol	Hombikat UV100	145 ppm	<0.65 mW/cm² (UV part)	>99% mineralization	Kirchnerova [46]
Ketones	Acetone	Synthesized TiO_2	450 ppmv	2.7 mW/cm²	100% conversion	Coronado [47]
Aromatics	Benzene	P25	<5 ppm	5 mW/cm²	100% conversion	Jacoby [48]
		P25	100 ppmv	5.7 mW/cm² UVC	100% conversion	Bouazza [49]
	Toluene	P25	0.45 g/m³	3.05 mW/cm² UVC	3.9 g/m²/h	Keshmiri [50]
		TiO_2, not specified	1043 mg/m³	*not specified,* UVC	100% conversion	Bouzaza [51]
	m-xylene	P25	*not specified trace*	5 x 10^{-7} E/cm²/min	0.2 µg/cm²/min	Peral [42]
	Phenol	P25	*not specified*; *adsorbed vapor*	*not specified for gas experiment*	Full conversion + mechanistic elucidation	Palmisano [52]
Dioxins [d]	1,2-dichlorobenzene	P25	3.9 mmol/Nm³	14.8 mW/cm²	~100% destruction and removal efficiency	Lu [53]
	2,3,7,8-tetrachlorodibenzo-p-dioxin	P25	500 ng/cm² on solid-gas interface	*not specified*	99.86% conversion	Wu [54]
	1,2,3,6,7,8-hexachlorodibenzo-p-dioxin	P25	12.5 ng/cm² on solid-gas interface	6.33 mW/cm²	100% conversion	Wu [55]

[a] all catalysts are TiO_2-based. This column mainly indicates if commercially available, or lab-made catalysts were used.

[b] given in the same units or terminology as reported in (or directly derived from) the corresponding reference

[c] either the conversion of the pollutant, the oxidation rate or a mechanistic insight, in the same units or terminology as reported in (or directly derived from) the corresponding reference

[d] including model compounds for dioxins

Table 2. ***Dimensionless ratio of several material and catalytic properties of PC500 and P25 for the gas phase PCO of acetaldehyde.***[a]

Property	**Ratio PC500/P25**
Turnover frequency (TOF)	1.3
Specific surface area	6.0
Acetaldehyde adsorbed	3.5
Absolute amount OH groups	3.75
Photocurrent	<0.01

[a] adapted from ref. [41] based on the original data